Aerospace Science and Technology 142 (2023) 108617

Contents lists available at ScienceDirect

Aerospace Science and Technology

journal homepage: www.elsevier.com/locate/aescte

Three-dimensional approximate cooperative integrated guidance and control with fixed-impact time and azimuth constraints

Zhibing Li [a], Xiaoyue Zhang [a,*], Huanrui Zhang [a], Feng Zhang [b]

[a] *School of Instrumentation and Optoelectronic Engineering, Beihang University, Beijing, 100191, China*
[b] *China North Industries Corp., Beijing, 100029, China*

A R T I C L E   I N F O

Article history:
Received 20 March 2023
Received in revised form 23 August 2023
Accepted 5 September 2023
Available online 11 September 2023
Communicated by Xiande Fang

Keywords:
Approximate cooperative integrated guidance and control
Fixed-impact time constraint
Fixed-impact azimuth constraint
3D reduced-order ESO

A B S T R A C T

A novel three-dimensional (3D) approximate cooperative integrated guidance and control (ACIGC) scheme based on backstepping control (BC), sliding mode control (SMC), dynamic surface control (DSC), and a 3D reduced-order extended state observer (ESO) for multiple hypersonic skid-to-turn (STT) missiles simultaneously attacking ground-maneuver targets is proposed in this study, which considers a fixed-impact azimuth and time constraints. First, we established a novel integrated guidance and control (IGC) model that includes the missile-target relative distance and azimuth based on the missile-target engagement dynamics, attitude dynamics, and first-order delay dynamics of the rudder. It is a 3D fifth-order strict-feedback time-varying nonlinear model with mismatched uncertainties. Second, a 3D ACIGC scheme was designed, where a cooperative strategy was designed by transforming a fixed-impact time constraint into a nominal range-to-go constraint. The IGC model consists of seeker, guidance, angle-of-attack, attitude, and rudder subsystems based on the BC, and the SMC designs each subsystem. The DSC obtains the derivatives of virtual control commands, which solves the "differential explosion" caused by the BC. The unknown target acceleration, unmodeled parts of the system states, perturbations caused by time-varying parameters, and external disturbances are regarded as lumped disturbances, which are estimated and compensated for by the 3D reduced-order ESO to improve the robustness. Subsequently, the closed-loop system was proven to be stable, and the system states were ultimately uniformly bounded using Lyapunov theory. Finally, the simulation results of three missiles attacking a simultaneously ground-maneuvering target and Monte Carlo simulations demonstrated the effectiveness and robustness of the proposed ACIGC scheme.

1. Introduction

Hypersonic missiles can effectively reduce the detection time of enemy radars and the response time of defense systems, owing to their fast flight speed and high maneuverability. This makes hypersonic missiles an effective weapon to attack key enemy targets. It can also complete various military missions with specific strategic deterrence significance such as surveillance, reconnaissance, and strike operations. Over the past decade, significant progress has been made in hypersonic aerodynamics, thermal protection, and scramjet technologies for hypersonic missiles [1]. The maneuverability and guidance accuracy of the hypersonic missiles improved significantly. However, the survivability and attack effectiveness of single missiles have weakened with recent improvements in the missile defense systems. Salvo attacks on multiple missiles have become an effective method to improve the possibility of penetration. The simultaneous attack of multiple missiles against a target can effectively increase the survivability of the missiles and the probability of destruction against the target, thus becoming the subject of this research topic.

The current research on multimissile salvo guidance and control algorithms can be divided into two categories. The first category is a simultaneous attack on the time scale, that is, the individual homing guidance mode that satisfies the fixed-impact time constraint. The advantage of this guidance strategy is that there is no dynamic information interaction between missiles during engagement, nor is there a communication topology required between the missiles, and thus it can be defined as approximate cooperation. This constitutes

* Corresponding author.
E-mail addresses: lizhibing@buaa.edu.cn (Z. Li), zhangxiaoyue@buaa.edu.cn (X. Zhang), zhanghr@buaa.edu.cn (H. Zhang), zhangfeng@norinco.cn (F. Zhang).

https://doi.org/10.1016/j.ast.2023.108617
1270-9638/

the open-loop guidance strategy. Because no communication link between missiles is required during missile-target engagement, multiple missiles can achieve simultaneous attacks when encountering electronic interference from the enemy. This guidance strategy is commonly used in guidance law designs with a fixed-impact-time constraint. A fixed-impact time-constrained guidance law (ITCG) was first applied in [2], where an ITCG was proposed for stationary targets based on the proportional guidance law (PNG) and desired impact-time error. Subsequently, many scholars have conducted studies on ITCG. In [3], an ITCG was proposed using a time-varying PNG and bias feedback command. The proposed time-to-go estimation based on time-varying PNG is more accurate than the time-to-go estimation calculated using conventional PNG. In [4], a three-stage PNG was proposed in [4], which achieved the impact-time constraint by designing different guidance constants to change the ballistic trajectory. Based on the impact-time constraint, many scholars have proposed guidance laws that satisfy other constraints such as the angle-of-attack [5] and field-of-view (FOV) constraints [6]. Based on an optimal control algorithm, [7] proposed an impact-angle-constrained guidance law and matched time-to-go estimation algorithm. It implements an impact-time constraint by adding a feedback control term. In [8], a two-stage guidance law was proposed to achieve impact time and angle constraints, where a switching strategy ensured the connection of the two-stage guidance law. Reference [9] proposed a guidance law that satisfied both the impact time and FOV constraints based on a time-varying sliding mode control (SMC), where the time-to-go estimation avoided the small-angle assumption. With PNG and biased PNG, [10] proposed a three-dimensional (3D) impact-time guidance law and simultaneously satisfied the FOV constraint, where the bias term ensured that the missile intercepted the target within the desired attack time. In literature [11], a 3D time-to-go estimation was proposed and the FOV constraint was achieved by adding a bias term to a 3D PNG.

The aforementioned studies were mainly conducted for stationary or slow-moving targets, and all relied on time-to-go estimation. However, it is difficult to accurately estimate time-to-go, particularly for maneuvering targets. If the time-to-go estimation has a large error, guidance strategies may fail and even lead to missing a target. Some studies have attempted to design guidance laws with impact-time constraints without using a time-to-go prediction formula. Reference [12] proposed a cruise guidance law that satisfied both the impact angle and time constraints and achieved the impact-time constraint by controlling the missile trajectory, thus avoiding the use of time-to-go prediction. Reference [13] proposed a guidance law based on two different nonsingular terminal sliding mode controls that satisfy the impact angle and time constraints. The time-to-go estimation was revised using the predicted intercept point to achieve interception of constant acceleration targets. Reference [14] achieved the desired impact time by tracking a time-varying line-of-sight (LOS) profile, which enabled a strike against a maneuvering target owing to the accurate estimation of the unknown acceleration of the target using the inertial-delay control method. In [15] a 3D guidance law was designed with an impact-time constraint for moving targets.

The second category is cooperative homing guidance, which achieves distance or position agreement with real-time communication topology between missiles. Specifically, in missile-target engagement, real-time data are transmitted between missiles through a communication topology. Each missile generates cooperative commands to achieve a simultaneous attack based on the position information of the adjacent missiles. The consensus of multiagent systems is often used to design cooperative guidance laws to achieve time-to-go or position agreement. Reference [16] proposed a 3D adaptive fixed-time cooperative guidance law with an impact angle constraint, where the fixed-time consensus theory was used to ensure agreement of the time-to-go estimation errors of missiles. Graph theory proved that communication topology switching failures did not affect the proposed guidance law. A cooperative guidance law considering the impact angle constraint was proposed in [17], in which a finite-time consensus protocol was used to design acceleration commands along the LOS to ensure that all missiles simultaneously attacked the maneuvering target. In the second stage, the acceleration commands in the direction normal to the LOS were designed based on the adaptive fast-terminal SMC to ensure the achievement of the impact angle constraint. A cooperative guidance law considering the FOV constraint was proposed by centralized and distributed communication topologies in the literature [18], where a centralized leader-follower structure was used for communication within the group and a distributed communication topology was used for communication between the leaders of each group. In [19], a 3D cooperative guidance law based on a distributed communication topology was proposed using the multiagent systems consensus theory to guarantee time-to-go agreement. In literature [20], a 3D cooperative guidance law with an impact angle constraint was proposed based on a distributed communication topology. The distributed sliding mode surface (SMS) required only state information from adjacent missiles, and the multiagent system consensus theory ensured the agreement of range-to-go for all missiles and avoided the estimation error of time-to-go. Reference [21] proposed a leader-follower cooperative guidance strategy in which only the leader missile is equipped with a seeker. The leader adopts a guidance law that satisfies the prespecified impact time, and the follower adopts a cooperative guidance law that ensures proportional consensus with the leader's range-to-go.

The aforementioned guidance strategies are primarily based on the relative motion of the missile-target, and derive normal overloads to achieve the impact-time constraint. The above guidance laws are designed under the assumption of spectral separation, that is, assuming that the dynamics of missiles are ideal or that the time constant of the control loop (autopilot) is much smaller than that of the guidance loop; thus, the control loop can be ignored in the design. However, the missile-target distance changes rapidly during the terminal guidance phase, and the dynamics of the missile control loop significantly affect the response time of the guidance loop. The traditional design method of separating guidance and control loops (SGC) may lead to performance degradation of the guidance control system, which may become unstable [22]. The integrated guidance and control (IGC) design method treats the guidance and control loops as a whole and derives control commands directly based on the missile-target motion relation and missile dynamics. It has been shown that the IGC method can fully exploit the coupling effect between the guidance and control loops compared to the SGC method, which is conducive to improving the stability of the entire guidance control system and reducing the miss distance [23]. Additionally, the IGC method can shorten the design cycle and improve economy and reliability [24]. For the cooperative integrated guidance and control (CIGC) design scheme with simultaneous attacks, some scholars have attempted to establish the dynamic characteristics of the time-to-go by missile time-to-go formulation and dynamics, establish the SMS with time-to-go estimation errors, and derive rudder control commands [25,26]. In [27], a missile time-to-go dynamic formulation was established. The leader-follower and no-leader modes were designed to determine whether the impact time was predefined or set in the engagement. The other category achieves a simultaneous attack by establishing a higher-order IGC model and then designing it using backstepping control (BC) and SMC. In [28], an IGC model with a target look angle was established. Subsequently, a simultaneous attack with a predefined impact time was achieved by tracking the error between the actual and nominal range-to-go. In [29], a 3D IGC model containing the heading error was established, and a partial integrated guidance and control approach was proposed, in which a simultaneous attack was achieved by tracking the average distance of all missiles. In [30], the desired lateral accelerations were derived using the bias-tracking guidance law. The virtual commands of the guidance loop are then accurately tracked by an autopilot to achieve a simultaneous attack with a predefined impact time. In [31], an IGC design scheme with an impact angle constraint was proposed, and a formulation was designed to estimate the impact time. This allows adjustment of the missile controller parameters to achieve a predefined impact time.

In summary, simultaneous attacks with a fixed-impact time were primarily considered in the guidance law design. However, the guidance law is usually designed with the assumption of ideal autopilot dynamic characteristics, which is equivalent to ignoring the autopilot dynamics. The characteristics of the terminal guidance phase of hypersonic missiles are fast time varying and strong disturbances, and the dynamic characteristics of the autopilot significantly affect the response speed of the missiles, which must be considered. The CIGC can fully consider the coupling effect between the guidance and control loops, thereby effectively improving the performance of the guidance control system. Most CIGC schemes with fixed-impact times have been designed based on missile time-to-go estimation. However, it is difficult to accurately estimate the time-to-go for maneuvering the targets. Therefore, when there was a large deviation between the estimated and actual time-to-go, the terminal-impact time also exhibited a large deviation. Moreover, most of the aforementioned CIGC schemes consider only the saturation input constraint and regard the controller output as the actual rudder angle; that is, the dynamic characteristics of the rudders are ideal and the delay dynamics of the rudders are neglected. As the only actuator in the terminal guidance phase of hypersonic missiles, the rudder delay dynamics also affect the response speed of the missile guidance control system and therefore needs to be considered in the design. Additionally, if multiple missiles can approach and attack the target at different azimuths, the probability of penetration is significantly enhanced, and the damaging effect is amplified. For all intents and purposes, the CIGC of hypersonic missiles attacking ground-maneuvering targets and considering the constraints of rudder delay dynamics and saturation, fixed-impact azimuth, and fixed-impact time has never been observed in previous studies.

Inspired by the above analysis, based on SMC, BC, dynamic surface control (DSC), and 3D reduced-order extended state observer (ESO), this study proposes a novel 3D ACIGC scheme with fixed-impact azimuth and fixed-impact time constraints for multiple hypersonic skid-to-turn (STT) missiles attacking a ground-maneuvering target, which only requires setting the same impact time and individual impact azimuth at the beginning of the terminal guidance. Moreover, to ensure robustness, the perturbations caused by variations in the aerodynamic parameters, unmodeled parts of the system states, external disturbances, and target maneuvers were regarded as lumped disturbances that were estimated using a 3D reduced-order ESO. Compared to the existing results on CIGC schemes, the main contributions of this study can be summarized as follows.

1) In contrast to the literature [13,25,27,30], the proposed 3D ACIGC scheme simultaneously considers the fixed-impact time, rudder delay dynamics and saturation, and impact azimuth constraints, which have not been simultaneously satisfied in previous studies.
2) In this study, a novel cooperative strategy was designed by transforming a fixed-impact time constraint into a nominal range-to-go constraint. Subsequently, a novel 3D strict-feedback nonlinear IGC model with mismatched uncertainties was established, containing the missile-target distance, missile-target azimuth, attitude dynamics equations of missiles, and a first-order delay model of the rudder.
3) A 3D ACIGC controller was designed based on SMC, BC, and DSC. First, based on the BC, the guidance control system consists of seeker, guidance, angle-of-attack, attitude, and rudder subsystems. The lumped disturbances in the system model are estimated and compensated for by the 3D reduced-order ESO to ensure the robustness of the proposed ACIGC scheme, which also avoids switching terms in the controller, thus avoiding the "chattering" caused by the SMC.
4) Lyapunov theory proves the stability of the closed-loop system and uniformly bounded system states. The numerical simulation results also proved the effectiveness and robustness of the proposed scheme.

The remainder of this paper is organized as follows. Section 2 presents the 3D IGC model derivation process and control objective design. Section 3 elaborates on the cooperative strategy and the 3D ACIGC scheme. The stability of the closed-loop system is described in Section 4. Section 5 presents the simulation results and data analysis. Finally, the conclusions of this study are summarized in Section 6.

2. Model design and control objectives

Aiming at hypersonic missiles attacking ground-maneuvering targets, a 3D nonlinear strict-feedback IGC model was established based on missile-target engagement kinematics, dynamic equations, and rudder first-order delay models. The design objectives of this study were as follows.

2.1. Problem formulation

The missile-target engagement geometry in a 3D space coordinate system is shown in Fig. 1. M and T denote the missile and the target, respectively. $Ox_Iy_Iz_I$ is an Earth-fixed inertial coordinate system. $Mx_Ly_Lz_L$ is the missile LOS coordinate system attached to the missile, where Mx_L is coincident with the LOS, and the positive direction points toward the target. My_L lies in the longitudinal plane containing the Mx_L axis, is perpendicular to the Mx_L axis, upwards is defined as positive. The Mz_L axis is perpendicular to the Mx_Ly_L plane, and follows the right-hand rule. The elevation and azimuth angles of the LOS are denoted as q_1 and q_2, respectively, and are defined counterclockwise as positive. The missile flight path and azimuth angles are denoted by θ_M and ψ_{VM}, respectively, and their counterclockwise directions are positive.

Assumption 1. For an easy modeling analysis, the missile can be simplified to a perfect point motion during engagement in the terminal guidance phase.

Assumption 2. In the terminal guidance phase, the missile thrust is zero and the velocity of the missile is constant. In other words, the variation in the missile velocity can be regarded as an unmodeled part of the system states.

The relative distance, velocity, and acceleration vectors between the missile and target are denoted as $\mathbf{R}$, $\mathbf{V}_R$, and $\mathbf{a}_R$, respectively. According to the Coriolis theorem, the following equations can be derived as follows:

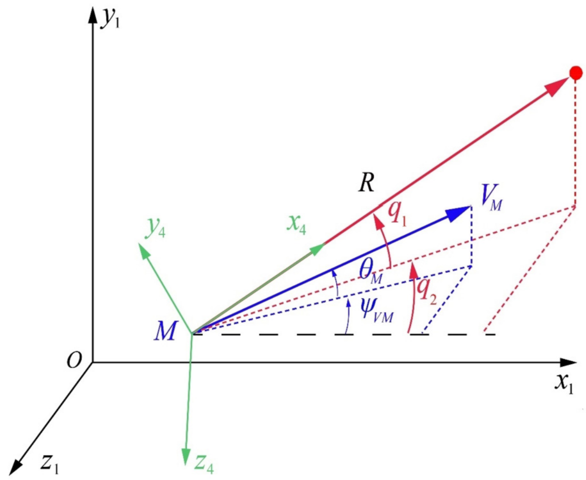

Fig. 1. Three-dimensional missile-target engagement geometry.

$$\mathbf{V_R} = \frac{\partial \mathbf{R}}{\partial t} + \boldsymbol{\Omega} \times \mathbf{R}, \tag{1}$$

$$\mathbf{a_R} = \frac{\partial \mathbf{V_R}}{\partial t} + \boldsymbol{\Omega} \times \mathbf{V_R}, \tag{2}$$

where $\mathbf{V}_R = [\,V_{Rx_L} \quad V_{Ry_L} \quad V_{Rz_L}\,]^T$, $\mathbf{R} = [\,R \quad 0 \quad 0\,]^T$, $\mathbf{a}_R = [\,a_{Rx_L} \quad a_{Ry_L} \quad {}_{Rz_L}\,]^T$. $\boldsymbol{\Omega} = [\dot{q}_2 \sin q_1 \dot{q}_2 \cos q_1 \dot{q}_1]^T$ is the angular velocity vector of the LOS coordinate system with respect to the inertial coordinate system.

Equation (1) can be derived as

$$\mathbf{V_R} = \begin{bmatrix} V_{Rx_L} \\ V_{Ry_L} \\ V_{Rz_L} \end{bmatrix} = \begin{bmatrix} \dot{R} \\ 0 \\ 0 \end{bmatrix} + \begin{bmatrix} 0 & \dot{q}_1 & \dot{q}_2 \cos q_1 \\ \dot{q}_1 & 0 & -\dot{q}_2 \sin q_1 \\ -\dot{q}_2 \cos q_1 & \dot{q}_2 \sin q_1 & 0 \end{bmatrix} \begin{bmatrix} R \\ 0 \\ 0 \end{bmatrix} = \begin{bmatrix} \dot{R} \\ R\dot{q}_1 \\ -R\dot{q}_2 \cos q_1 \end{bmatrix}. \tag{3}$$

Substituting Eq. (3) into Eq. (2) yields

$$\mathbf{a}_R = \mathbf{a}_{T_L} - \mathbf{a}_{M_L} = \begin{bmatrix} a_{Tx_L} \\ a_{Ty_L} \\ a_{Tz_L} \end{bmatrix} - \begin{bmatrix} a_{Mx_L} \\ a_{My_L} \\ a_{Mz_L} \end{bmatrix} = \begin{bmatrix} \ddot{R} - R\dot{q}_1^2 - R\dot{q}_2^2 \cos^2 q_1 \\ 2\dot{R}\dot{q}_1 + R\ddot{q}_1 + R\dot{q}_2^2 \sin q_1 \cos q_1 \\ -R\ddot{q}_2 \cos q_1 - 2\dot{R}\dot{q}_2 \cos q_1 + 2R\dot{q}_1\dot{q}_2 \sin q_1 \end{bmatrix}, \tag{4}$$

where $\mathbf{a}_{T_L} = \left[a_{Tx_L}, a_{Ty_L}, a_{Tz_L}\right]^T$ and $\mathbf{a}_{M_L} = \left[a_{Mx_L}, a_{My_L}, a_{Mz_L}\right]^T$ denote the acceleration vectors of the target and missile in the LOS coordinate system, respectively.

The velocity vector of the missile $\mathbf{V}_M$ in the inertial coordinate system is expressed as follows:

$$\mathbf{V}_M = \begin{bmatrix} V_{Mx} \\ V_{My} \\ V_{Mz} \end{bmatrix} = \begin{bmatrix} V_M \cos\theta_M \cos\psi_{VM} \\ V_M \sin\theta_M \\ -V_M \cos\theta \sin\psi_{VM} \end{bmatrix}. \tag{5}$$

According to the geometry between the inertial coordinate system and the LOS coordinate system, the coordinate transformation matrix can be obtained as

$$L\left(q_2, q_1\right) = \begin{bmatrix} \cos q_1 \cos q_2 & \sin q_1 & -\cos q_1 \sin q_2 \\ -\sin q_1 \cos q_2 & \cos q_1 & \sin q_1 \sin q_2 \\ \sin q_2 & 0 & \cos q_2 \end{bmatrix}. \tag{6}$$

Therefore, the velocity vector of the missile in the LOS coordinate system can be derived as

$$\mathbf{V}_{M_L} = L\left(q_2, q_1\right) \mathbf{V}_M = \begin{bmatrix} V_{Mx_L} \\ V_{My_L} \\ V_{Mz_L} \end{bmatrix} = \begin{bmatrix} V_M \cos\theta_M \cos q_1 \cos\left(q_2 - \psi_{VM}\right) + V \sin\theta_M \sin q_1 \\ -V_M \cos\theta_M \sin q_1 \cos\left(q_2 - \psi_{VM}\right) + V \sin\theta_M \cos q_1 \\ V_M \cos\theta_M \sin\left(q_2 - \psi_{VM}\right) \end{bmatrix}. \tag{7}$$

According to the Coriolis theorem, the missile acceleration vector in the LOS coordinate system can be expressed as

$$\mathbf{a}_{M_L} = \frac{\partial \mathbf{V}_{M_L}}{\partial t} + \boldsymbol{\Omega} \times \mathbf{V}_{M_L}. \tag{8}$$

Substituting Eq. (7) into Eq. (8) yields

$$\mathbf{a}_{M_L} = \begin{bmatrix} a_{Mx_L} \\ a_{My_L} \\ a_{Mz_L} \end{bmatrix} = \begin{bmatrix} V_M\dot{\theta}_M \left[\cos\theta_M \sin q_1 - \sin\theta_M \cos q_1 \cos\left(q_2 - \psi_{VM}\right)\right] \\ +V_M \cos\theta_M \dot{\psi}_{VM} \cos q_1 \sin\left(q_2 - \psi_{VM}\right) \\ V_M\dot{\theta}_M \left[\cos\theta_M \cos q_1 + \sin\theta_M \sin q_1 \cos\left(q_2 - \psi_{VM}\right)\right] \\ -V_M \cos\theta_M \dot{\psi}_{VM} \sin q_1 \sin\left(q_2 - \psi_{VM}\right) \\ -V_M\dot{\theta}_M \sin\theta_M \sin\left(q_2 - \psi_{VM}\right) - V_M \cos\theta_M \dot{\psi}_{VM} \cos\left(q_2 - \psi_{VM}\right) \end{bmatrix}. \tag{9}$$

Substituting Eq. (9) into Eq. (4) yields

$$\begin{aligned}\ddot{R} =& R\dot{q}_1^2 + R\dot{q}_2^2\cos^2 q_1 - V_M\dot{\theta}_M\left[\cos\theta_M\sin q_1 - \sin\theta_M\cos q_1\cos(q_2-\psi_{VM})\right]\\ &- V_M\cos\theta_M\dot{\psi}_{VM}\cos q_1\sin(q_2-\psi_{VM}) + a_{Tx_L}\end{aligned}, \tag{10}$$

$$\begin{aligned}\ddot{q}_1 =& -\frac{2\dot{R}\dot{q}_1}{R} - \dot{q}_2^2\sin q_1\cos q_1 - \frac{V_M\dot{\theta}_M}{R}\left[\cos\theta_M\cos q_1 + \sin\theta_M\sin q_1\cos(q_2-\psi_{VM})\right]\\ &+ \frac{V_M\cos\theta_M\dot{\psi}_{VM}}{R}\sin q_1\sin(q_2-\psi_{VM}) + \frac{a_{Ty_L}}{R}\end{aligned}, \tag{11}$$

$$\begin{aligned}\ddot{q}_2 =& -\frac{2\dot{R}\dot{q}_2}{R} + 2\dot{q}_1\dot{q}_2\tan q_1 - \frac{V_M\dot{\theta}_M}{R\cos q_1}\sin\theta_M\sin(q_2-\psi_{VM})\\ &- \frac{V_M\cos\theta_M\dot{\psi}_{VM}}{R\cos q_1}\cos(q_2-\psi_{VM}) - \frac{a_{Tz_L}}{R\cos q_1}\end{aligned}. \tag{12}$$

The dynamics equation of the missile can be expressed as

$$\begin{cases}\dot{\theta}_M = \dfrac{Y\cos\gamma_V - Z\sin\gamma_V - mg\cos\theta_M}{mV_M}\\ \dot{\psi}_{VM} = \dfrac{-Y\sin\gamma_V - Z\cos\gamma_V}{mV_M\cos\theta_M}\end{cases}, \tag{13}$$

where Y and Z are the lift and side forces, respectively. γ_V is the velocity-deflection angle. m is the missile mass. V_M denote the missile velocity.

Assumption 3. For STT missiles, one control objective is to maintain γ_V stabilized near zero to ensure flight stability. That is, γ_V can be reasonably approximated as $\sin\gamma_V \approx 0$, $\cos\gamma_V \approx 1$.

Define $f_{R1} = \cos\theta_M\sin q_1 - \sin\theta_M\cos q_1\cos(q_2-\psi_{VM})$, $f_{R2} = \cos q_1\sin(q_2-\psi_{VM})$, $f_{\varepsilon 1} = [\cos\theta_M\cos q_1 + \sin\theta_M\sin q_1\cos(q_2-\psi_{VM})]/R$, $f_{\varepsilon 2} = \sin q_1\sin(q_2-\psi_{VM})/R$, $f_{\eta 1} = \dfrac{\sin\theta_M\sin(q_2-\psi_{VM})}{R\cos q_1}$, $f_{\eta 2} = \dfrac{\cos(q_2-\psi_{VM})}{R\cos q_1}$. According to Assumption 3, by substituting Eq. (13) into Eqs. (10)–(12) yields

$$\ddot{R} = R\dot{q}_1^2 + R\dot{q}_2^2\cos^2 q_1 - f_{R1}\frac{Y - mg\cos\theta_M}{m} + f_{R2}\frac{Z}{m} + a_{Tx_L}, \tag{14}$$

$$\ddot{q}_1 = -\frac{2\dot{R}\dot{q}_1}{R} - \dot{q}_2^2\sin q_1\cos q_1 - f_{\varepsilon 1}\frac{Y - mg\cos\theta_M}{m} - f_{\varepsilon 2}\frac{Z}{m} + \frac{a_{Ty_L}}{R}, \tag{15}$$

$$\ddot{q}_2 = -\frac{2\dot{R}\dot{q}_2}{R} + 2\dot{q}_1\dot{q}_2\tan q_1 - f_{\eta 1}\frac{Y - mg\cos\theta_M}{m} + f_{\eta 2}\frac{Z}{m} - \frac{a_{Tz_L}}{R\cos q_1}. \tag{16}$$

The aerodynamic forces and aerodynamic moments of missiles can be approximated as

$$\begin{cases}Y = c_y^{\alpha} QS\alpha + d_Y\\ Z = c_z^{\beta} QS\beta + d_Z\end{cases}, \tag{17}$$

$$\begin{cases}M_x = \left(m_x^{\alpha}\alpha + m_x^{\beta}\beta + m_x^{\delta_x}\delta_x\right)QSL + d_{M_x}\\ M_y = \left(m_y^{\beta}\beta + m_y^{\delta_y}\delta_y\right)QSL + d_{M_y}\\ M_z = \left(m_z^{\alpha}\alpha + m_z^{\delta_z}\delta_z\right)QSL + d_{M_z}\end{cases}, \tag{18}$$

where d_Y, d_Z, d_{M_x}, d_{M_y}, and d_{M_z} are the aerodynamic parameter errors due to the approximation. M_x, M_y and M_z are the roll, yaw, and pitch moments, respectively. c_i^j $(i = y, z;\ j = \alpha, \beta)$ denote the derivatives of force coefficients with respect to α and β. α is the angle of attack, and β is the sideslip angle. m_i^j $(i = x, y, z;\ j = \alpha, \beta)$ are the moment coefficients. $Q = \frac{1}{2}\rho V_m^2$ is the dynamic pressure and ρ is the atmospheric density. S and L denote the reference area and length, respectively. δ_x, δ_y and δ_z denote the aileron, rudder and elevator deflections, respectively.

Substituting Eq. (17) into Eqs. (14)–(16) yields

$$\ddot{R} = R\dot{q}_1^2 + R\dot{q}_2^2\cos^2 q_1 + f_{R1}g\cos\theta_M - f_{R1}\frac{c_Y^{\alpha}QS\alpha}{m} + f_{R2}\frac{c_Z^{\beta}QS\beta}{m} + \Delta_R, \tag{19}$$

$$\ddot{q}_1 = -\frac{2\dot{R}\dot{q}_1}{R} - \dot{q}_2^2\sin q_1\cos q_1 + f_{\varepsilon 1}g\cos\theta_M - f_{\varepsilon 1}\frac{c_Y^{\alpha}QS\alpha}{m} - f_{\varepsilon 2}\frac{c_Z^{\beta}QS\beta}{m} + \Delta_{q_1}, \tag{20}$$

$$\ddot{q}_2 = -\frac{2\dot{R}\dot{q}_2}{R} + 2\dot{q}_1\dot{q}_2\tan q_1 + f_{\eta 1}g\cos\theta_M - f_{\eta 1}\frac{c_Y^{\alpha}QS\alpha}{m} + f_{\eta 2}\frac{c_Z^{\beta}QS\beta}{m} + \Delta_{q_2}. \tag{21}$$

The attitude dynamics equation of the missile can be given as

$$\begin{cases} \dot{\alpha} = -\omega_x \tan\beta \cos\alpha + \omega_y \tan\beta \sin\alpha + \omega_z \\ \qquad - \dfrac{Y}{mV_M \cos\beta} + \dfrac{g\cos\theta_M \cos\gamma_V}{V_M \cos\beta} + d_\alpha \\ \dot{\beta} = \omega_x \sin\alpha + \omega_y \cos\alpha + \dfrac{Z}{mV_M} + \dfrac{g\cos\theta_M \sin\gamma_V}{V_M} + d_\beta \\ \dot{\gamma}_V = \omega_x \cos\alpha \sec\beta - \omega_y \sin\alpha \sec\beta - \dfrac{g\cos\theta_M \cos\gamma_V \tan\beta}{V_M} \\ \qquad + \dfrac{Y(\tan\theta_M \sin\gamma_v + \tan\beta) + Z\tan\theta_M \cos\gamma_v}{mV_M} + d_{\gamma_V} \end{cases}, \tag{22}$$

$$\begin{cases} \dot{\omega}_x = \dfrac{J_y - J_z}{J_x}\omega_z\omega_y + \dfrac{M_x}{J_x} + d_{\omega_x} \\ \dot{\omega}_y = \dfrac{J_z - J_x}{J_y}\omega_x\omega_z + \dfrac{M_y}{J_y} + d_{\omega_y} \\ \dot{\omega}_z = \dfrac{J_x - J_y}{J_z}\omega_y\omega_x + \dfrac{M_z}{J_z} + d_{\omega_z} \end{cases}. \tag{23}$$

where ω_x, ω_y and ω_z denote the roll, yaw, and pitch rates, respectively. d_α, d_β, d_{γ_V}, d_{ω_x}, d_{ω_y} and d_{ω_z} represent the modeling error terms caused by omitting higher order terms and time-varying perturbation errors of aerodynamic parameters.

If the missile rudder is simplified to a first-order system, the rudder model can be expressed as follows

$$\begin{aligned} \delta_{xc} &= \tau_x\dot{\delta}_x + \delta_x \\ \delta_{yc} &= \tau_y\dot{\delta}_y + \delta_y, \\ \delta_{zc} &= \tau_z\dot{\delta}_z + \delta_z \end{aligned} \tag{24}$$

where δ_{xc}, δ_{yc} and δ_{zc} denote the control inputs of aileron, rudder and elevator channel, respectively. τ_x, τ_y and τ_z denote the time constant of the aileron, rudder and elevator channel, respectively.

Owing to the physical limitations of the rudder, the controller commands should satisfy the following saturation function to ensure that the rudder amplitudes do not exceed the maximum limit.

$$sat(\delta_{ic}) = \begin{cases} \delta_i^{\max} sign(\delta_{ic}), & |\delta_{ic}| > \delta_i^{\max} \\ \delta_{ic}, & |\delta_{ic}| \le \delta_i^{\max} \end{cases} \quad i = x, y, z \tag{25}$$

where $\delta_i^{\max}$ $(i = x, y, z)$ are upper-bounds of the deflections.

Based on the assumptions above and model approximations, Eqs. (19)–(25), the 3D nonlinear strict-feedback IGC model with mismatched uncertainties can be summarized as follows:

$$\begin{cases} \dot{\mathbf{x}}_0 = \mathbf{x}_1 \\ \dot{\mathbf{x}}_1 = \mathbf{F}_1 + \mathbf{G}_1\mathbf{x}_2^* + \mathbf{d}_1 \\ \dot{\mathbf{x}}_2 = \mathbf{F}_2 + \mathbf{G}_2\mathbf{x}_3 + \mathbf{d}_2 \\ \dot{\mathbf{x}}_3 = \mathbf{F}_3 + \mathbf{G}_3\mathbf{x}_4 + \mathbf{d}_3 \\ \dot{\mathbf{x}}_4 = \mathbf{F}_4 + \mathbf{G}_4\,\mathrm{sat}(\mathbf{u}) \end{cases}, \tag{26}$$

where the system state vectors are $\mathbf{x}_0 = [R, q_2]^T$, $\mathbf{x}_1 = [\dot{R}, \dot{q}_2]^T$, $\mathbf{x}_2^* = [\alpha, \beta]^T$, $\mathbf{x}_2 = [\alpha, \beta, \gamma_V]^T$, $\mathbf{x}_3 = [\omega_x, \omega_y, \omega_z]^T$ and $\mathbf{x}_4 = [\delta_x, \delta_y, \delta_z]^T$. The control input vector is $\mathbf{u} = [\delta_{xc}, \delta_{yc}, \delta_{zc}]^T$. $\mathbf{d}_1$, $\mathbf{d}_2$, and $\mathbf{d}_3$ are lumped disturbances. The remaining nonlinear functions are expressed as

$$\mathbf{F}_1 = \begin{bmatrix} R\dot{q}_1^2 + R\dot{q}_2^2\cos^2 q_1 + f_{R1}g\cos\theta_M \\ -\dfrac{2\dot{R}\dot{q}_2}{R} + 2\dot{q}_1\dot{q}_2\tan q_1 + f_{\eta 1}g\cos\theta_M \end{bmatrix}^T,$$

$$\mathbf{G}_1 = \begin{bmatrix} -f_{R1}\dfrac{c_y^\alpha QS}{m} & f_{R2}\dfrac{c_z^\beta QS}{m} \\ -f_{\eta 1}\dfrac{c_y^\alpha QS}{m} & f_{\eta 2}\dfrac{c_z^\beta QS}{m} \end{bmatrix}^T,$$

$$\mathbf{F}_2 = \begin{bmatrix} -\dfrac{Y}{mV_M\cos\beta} + \dfrac{g\cos\theta_M\cos\gamma_V}{V_M\cos\beta} \\ \dfrac{Z}{mV_M} + \dfrac{g\cos\theta_M\sin\gamma_V}{V_M} \\ -\dfrac{g\cos\theta_M\cos\gamma_V\tan\beta}{V_M} + \dfrac{Z\tan\theta_M\cos\gamma_V + Y(\tan\theta_M\sin\gamma_v + \tan\beta)}{mV_M} \end{bmatrix}^T,$$

$$\mathbf{G}_2 = \begin{bmatrix} -\tan\beta\cos\alpha & \tan\beta\sin\alpha & 1 \\ \sin\alpha & \cos\alpha & 0 \\ \cos\alpha\sec\beta & -\sin\alpha\sec\beta & 0 \end{bmatrix}^T,$$

$$\mathbf{F}_3 = \begin{bmatrix} \dfrac{J_y - J_z}{J_x}\omega_z\omega_y + \dfrac{QSL\left(m_x^{\alpha}\alpha + m_x^{\beta}\beta\right)}{J_x} \\ \dfrac{(J_z - J_x)\,\omega_x\omega_z}{J_y} + \dfrac{QSLm_y^{\beta}\beta}{J_y} \\ \dfrac{\left(J_x - J_y\right)\omega_y\omega_x}{J_z} + \dfrac{QSLm_z^{\alpha}\alpha}{J_z} \end{bmatrix}^T,$$

$$\mathbf{G}_3 = QSL\begin{bmatrix} \dfrac{m_x^{\delta_x}}{J_x} & 0 & 0 \\ 0 & \dfrac{m_y^{\delta_y}}{J_y} & 0 \\ 0 & 0 & \dfrac{m_z^{\delta_z}}{J_z} \end{bmatrix}^T,$$

$$\mathbf{F}_4 = \begin{bmatrix} -\dfrac{1}{\tau_x}\delta_x \\ -\dfrac{1}{\tau_y}\delta_y \\ -\dfrac{1}{\tau_z}\delta_z \end{bmatrix}^T,$$

$$\mathbf{G}_4 = \begin{bmatrix} \dfrac{1}{\tau_x} & 0 & 0 \\ 0 & \dfrac{1}{\tau_y} & 0 \\ 0 & 0 & \dfrac{1}{\tau_z} \end{bmatrix}^T.$$

The errors between the saturation function and actual control command can be expressed as $\text{sat}(\mathbf{u}) = \mathbf{u} + \Delta\mathbf{u}$. Substituting this into the fifth equation of Eq. (26) yields

$$\begin{aligned} \dot{\mathbf{x}}_4 &= \mathbf{F}_4 + \mathbf{G}_4\,\text{sat}(\mathbf{u}) \\ &= \mathbf{F}_4 + \mathbf{G}_4(\mathbf{u} + \Delta\mathbf{u}). \\ &= \mathbf{F}_4 + \mathbf{G}_4\mathbf{u} + \mathbf{d}_4 \end{aligned} \tag{27}$$

Remark 1. $\mathbf{d}_1$ is primarily affected by the time-varying perturbation errors of the aerodynamic parameters and target maneuvers. $\mathbf{d}_2$ and $\mathbf{d}_3$ mainly contain the time-varying perturbation errors of the aerodynamic parameters and unmodeled parts of the system states. $\mathbf{d}_4$ mainly contains errors caused by the saturation function and rudder actuation.

Remark 2. Owing to the continuous and bounded aerodynamic parameters of the missile as well as the maneuverability of the target, the lumped disturbances of the system are also continuous and bounded.

Assumption 4. The system-lumped disturbances $\mathbf{d}_i,\ i = 1, 2, 3, 4$ and their derivatives are continuous and bounded; however, their upper boundaries are unknown.

Assumption 5. There is $\dot{R}(t) < 0$ in the terminal guidance phase. Moreover, since the missile and target have a non-zero size, there exist positive numbers $R_{\min}$ and $R_{\max}$ satisfying $R_{\min} < R(t_f) < R_{\max}$ at the interception point, and $R(t_f)$ is the distance between the missile and the target at the interception point.

2.2. Design objectives

For hypersonic STT missiles, in addition to satisfying the saturation constraint and rudder delay dynamics, the IGC controller for the strict-feedback IGC model proposed in Eqs. (26) and (27) should satisfy the following design objectives:

a) The miss distance should be less than 1 m.
b) The error between the impact time of each missile and predefined impact time should be less than 0.1 s.
c) The error between the terminal azimuth of each missile and the predefined azimuth was less than 1°.
d) The designed ACIGC scheme must be robust in the presence of unknown lumped disturbances.

3. Design of three-dimensional approximate cooperative integrated guidance and control

In this section, a 3D ACIGC scheme that considers the fixed-impact azimuth and fixed-impact time constraints is proposed. The 3D IGC model Eqs. (26) and (27) are time-varying nonlinear fifth-order strict-feedback systems with mismatched uncertainties: The BC consists

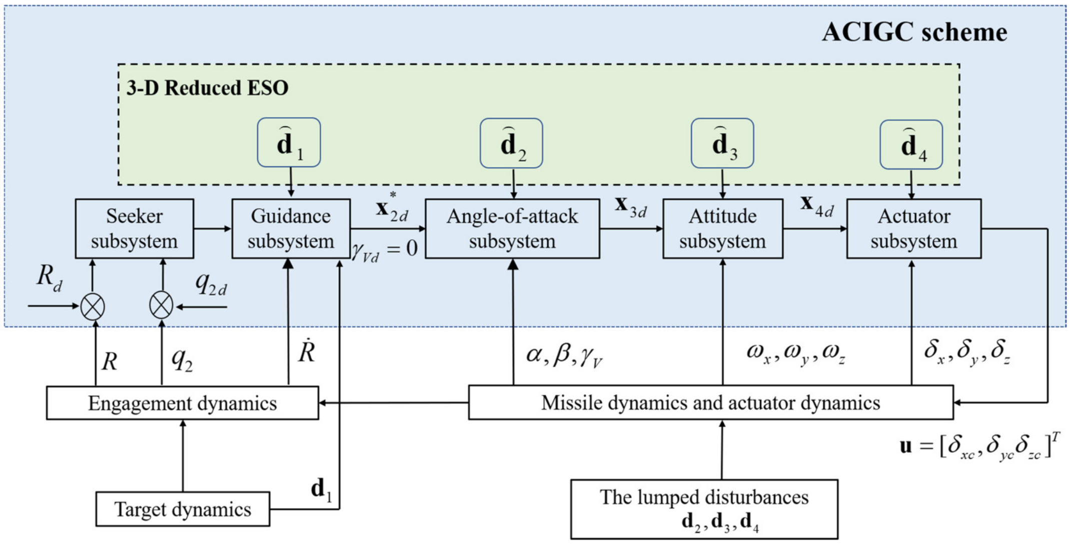

Fig. 2. Schematic diagram of the 3-D ACIGC.

of seeker, guidance, angle-of-attack, attitude, and rudder subsystems. Subsequently, each subsystem was designed using the SMC. The "differential explosion" phenomenon caused by the BC is solved by introducing the DSC. To ensure robustness, the lumped disturbances in the system were estimated using a 3D reduced-order ESO and compensated for in the control law. The designed ACIGC control scheme is shown in Fig. 2.

The following vector calculations were performed to facilitate the derivation of the formula: For vectors $\mathbf{a}=[a_1,a_2,\cdots,a_n]^T$ and $\mathbf{b}=[b_1,b_2,\cdots,b_n]^T$, we have

$$
\begin{aligned}
&\dot{\mathbf{a}}=[\dot{a}_1,\dot{a}_2,\cdots,\dot{a}_n]^T,\\
&\mathbf{a}^{\cdot\mathbf{b}}=[a_1^{b_1},a_2^{b_2},\cdots,a_n^{b_n}]^T,\\
&\mathbf{a}./\mathbf{b}=[a_1/b_1,a_2/b_2,\cdots,a_n/b_n]^T,\\
&\mathrm{sgn}^{\delta}(\mathbf{a})=[|a_1|^{\delta}\,\mathrm{sign}(a_1),|a_2|^{\delta}\,\mathrm{sign}(a_2),\cdots,|a_n|^{\delta}\,\mathrm{sign}(a_n)]^T,\\
&\mathrm{diag}(\mathbf{a}./\mathbf{b})=\mathrm{diag}(a_1/b_1,a_2/b_2,\cdots,a_n/b_n).
\end{aligned}
$$

3.1. Design of cooperative strategy

Simultaneous attacks based on a predefined time require multiple missiles to simultaneously hit a target. The design process is explained below, using a missile as an example. Assuming that the desired impact time is T_d, the nominal range-to-go can be defined as:

$$R_d=\gamma V_M\left(T_d-t\right), \tag{28}$$

where t is the current time and $0<\gamma<1$ is the cooperative coefficient to be designed.

As evident from Eq. (28), the nominal range-to-go is zero during $t=T_d$. When $t=0$, the initial nominal range-to-go value $R_{d0}=\gamma V_m T_d$. Based on the assumption that V_M is a constant, the initial nominal range-to-go value R_{d0} is decided by γ and T_d. The value of R_{d0} should be greater than the maximum initial missile-target distance of all missiles.

Differentiating Eq. (28) yields

$$\dot{R}_d=-\gamma V_m \tag{29}$$

From Eq. (29), it can be obtained that the rate of the nominal range-to-go is only related to γ. Define the angle between the missile velocity and line-of-sight as the missile leading angle η, then the rate of missile-target distance satisfies $\dot{R}=-V_M\cos\eta$ without considering the target motion. By changing the η, the missile can adjust $\dot{R}$, so that the missile-target distance R converges to R_d. In other words, the missile has $\dot{R}\geq\dot{R}_d$ throughout the terminal guidance phase. After R converges to R_d, the missile needs to satisfy $-V_M\cos\eta\approx\dot{R}_d$ to ensure that R accurately tracks R_d. Moreover, the smaller the η, the more stable the flight of the missile. Therefore, γ is selected related to the sine of the missile lead angle, and satisfies $0<\gamma<1$.

If each missile can make its distance to the target track an error within the nominal range-to-go ratio by controlling the rudder angle, then a simultaneous attack can be achieved within a predefined impact time. Hence, the fixed-impact time constraint is transformed into a missile-target distance constraint.

Moreover, we assumed that each missile could attack a target at its predefined azimuth at the interception point by controlling the rudder angle. In this case, it can achieve a multidirectional attack on the target, thereby enhancing the attack efficiency and increasing the damage effect.

If the desired attack azimuth is denoted as q_{2d}, redefining the system states $\mathbf{x}_0=[R-R_d,q_2-q_{2d}]^T$ and $\mathbf{x}_1=[\dot{R}-\dot{R}_d,\dot{q}_2-\dot{q}_{2d}]^T$, the first and second equations in Eq. (26) can be rewritten as

$$\begin{cases} \dot{\mathbf{x}}_0 = \mathbf{x}_1 \\ \dot{\mathbf{x}}_1 = \mathbf{F}_1 + \mathbf{G}_1 \mathbf{x}_2^* + \mathbf{d}_1 \end{cases}, \tag{30}$$

where

$$\mathbf{F}_1 = \begin{bmatrix} R\dot{q}_1^2 + R\dot{q}_2^2 \cos^2 q_1 + f_{R1} g \cos\theta_M - \ddot{R}_d \\ -\dfrac{2\dot{R}\dot{q}_2}{R} + 2\dot{q}_1\dot{q}_2 \tan q_1 + f_{\eta 1} g \cos\theta_M - \ddot{q}_{2d} \end{bmatrix}^T,$$

$$\mathbf{G}_1 = \begin{bmatrix} -f_{R1}\dfrac{c_Y^\alpha Q S}{m} & f_{R2}\dfrac{c_Z^\beta Q S}{m} \\ -f_{\eta 1}\dfrac{c_Y^\alpha Q S}{m} & f_{\eta 2}\dfrac{c_Z^\beta Q S}{m} \end{bmatrix}^T.$$

3.2. Design of IGC controller

In this section, each subsystem is designed based on SMC, DSC, and 3D reduced-order ESO.

Step 1: For the seeker subsystem, the first SMS is defined as

$$\mathbf{s}_0 = \mathbf{x}_0. \tag{31}$$

Differentiating Eq. (31), and combining Eq. (30) yields

$$\dot{\mathbf{s}}_0 = \dot{\mathbf{x}}_0 = \mathbf{x}_1. \tag{32}$$

Choosing $\mathbf{x}_1$ as the virtual control command that can be designed as follows:

$$\mathbf{x}_{1c} = -\mathbf{k}_0 \mathbf{s}_0, \tag{33}$$

where $\mathbf{k}_0 = \mathrm{diag}(k_{01}, k_{02})$ is a positive diagonal matrix.

The DSC is adopted so that $\mathbf{x}_{1c}$ is passed through a first-order–low-pass filter to obtain $\mathbf{x}_{1d}$ and $\dot{\mathbf{x}}_{1d}$ to avoid the "differential explosion" caused by the BC.

$$\begin{cases} \boldsymbol{\tau}_1 \dot{\mathbf{x}}_{1d} + \mathbf{x}_{1d} = \mathbf{x}_{1c} \\ \mathbf{x}_{1d}(0) = \mathbf{x}_{1c}(0) \end{cases}, \tag{34}$$

where $\boldsymbol{\tau}_1 = \mathrm{diag}(\tau_{11}, \tau_{12})$ is a filter time constant matrix.

Step 2: To ensure that the guidance subsystem tracks the virtual control commands of the seeker subsystem, the second SMS is defined as follows:

$$\mathbf{s}_1 = \mathbf{x}_1 - \mathbf{x}_{1d}. \tag{35}$$

Differentiating Eq. (35), and combining Eq. (30) yields

$$\begin{aligned} \dot{\mathbf{s}}_1 &= \dot{\mathbf{x}}_1 - \dot{\mathbf{x}}_{1d} \\ &= \mathbf{F}_1 + \mathbf{G}_1 \mathbf{x}_2^* + \mathbf{d}_1 - \dot{\mathbf{x}}_{1d} \end{aligned}. \tag{36}$$

Choosing $\mathbf{x}_2^*$ as the virtual control command that can be designed as follows:

$$\mathbf{x}_{2c}^* = \mathbf{G}_1^{-1}\left[-\mathbf{F}_1 - \hat{\mathbf{d}}_1 + \dot{\mathbf{x}}_{1d} - \mathbf{k}_1 \mathbf{s}_1\right], \tag{37}$$

where $\mathbf{k}_1 = \mathrm{diag}(k_{11}, k_{12})$ is the positive diagonal matrix. $\hat{\mathbf{d}}_1$ is the estimate of $\mathbf{d}_1$.

$\mathbf{x}_{2c}^*$ is continuous and has no switching term; thus, the chattering caused by the traditional SMC can be avoided.

$\mathbf{x}_{2d}^*$ and $\dot{\mathbf{x}}_{2d}^*$ are obtained by passing $\mathbf{x}_{2c}^*$ through a first-order–low-pass filter.

$$\begin{cases} \boldsymbol{\tau}_2 \dot{\mathbf{x}}_{2d}^* + \mathbf{x}_{2d}^* = \mathbf{x}_{2c}^* \\ \mathbf{x}_{2d}^*(0) = \mathbf{x}_{2c}^*(0) \end{cases}, \tag{38}$$

where $\boldsymbol{\tau}_2 = \mathrm{diag}(\tau_{21}, \tau_{22})$ is a filter time constant diagonal matrix.

Step 3∼5: The desired velocity-deflection angle of the missile should be zero to ensure flight stability of the STT missile. Therefore, it can be made that $\mathbf{x}_{2d} = [\mathbf{x}_{2d}^*, 0]^T$.

Similarly, for the angle-of-attack, attitude and rudder subsystems, the corresponding SMS can be defined as follows:

$$\mathbf{s}_i = \mathbf{x}_i - \mathbf{x}_{id},\ i = 2, 3, 4. \tag{39}$$

Differentiating Eq. (39) and combining the third equation in Eqs. (26) and (27) yields

$$\begin{aligned}\dot{\mathbf{s}}_i &= \dot{\mathbf{x}}_i - \dot{\mathbf{x}}_{id} \\ &= \mathbf{F}_i + \mathbf{G}_i\mathbf{x}_{i+1} + \mathbf{d}_i - \dot{\mathbf{x}}_{id}\end{aligned}, \tag{40}$$

where $\mathbf{x}_5 = \mathbf{u}$.

The corresponding virtual control commands and ACIGC control law can be designed as follows:

$$\mathbf{x}_{3c} = \mathbf{G}_2^{-1}[-\mathbf{F}_2 - \hat{\mathbf{d}}_2 + \dot{\mathbf{x}}_{2d} - \mathbf{k}_2\mathbf{s}_2], \tag{41}$$

$$\mathbf{x}_{4c} = \mathbf{G}_3^{-1}[-\mathbf{F}_3 - \hat{\mathbf{d}}_3 + \dot{\mathbf{x}}_{3d} - \mathbf{k}_3\mathbf{s}_3], \tag{42}$$

$$\mathbf{u} = \mathbf{G}_4^{-1}[-\mathbf{F}_4 - \hat{\mathbf{d}}_4 + \dot{\mathbf{x}}_{4d} - \mathbf{k}_4\mathbf{s}_4], \tag{43}$$

where $\mathbf{k}_2 = diag(k_{21}, k_{22}, k_{23})$, $\mathbf{k}_3 = diag(k_{31}, k_{32}, k_{33})$, and $\mathbf{k}_4 = diag(k_{41}, k_{42}, k_{43})$ are the positive diagonal matrixes. $\hat{\mathbf{d}}_2$, $\hat{\mathbf{d}}_3$, and $\hat{\mathbf{d}}_4$ are the estimates of $\mathbf{d}_2$, $\mathbf{d}_3$, and $\mathbf{d}_4$, respectively.

The first-order–low-pass filter used to obtain $\mathbf{x}_{3d}$, $\dot{\mathbf{x}}_{3d}$, $\mathbf{x}_{4d}$, and $\dot{\mathbf{x}}_{4d}$ can be formulated as follows:

$$\begin{cases}\boldsymbol{\tau}_3\dot{\mathbf{x}}_{3d} + \mathbf{x}_{3d} = \mathbf{x}_{3c} \\ \mathbf{x}_{3d}(0) = \mathbf{x}_{3c}(0)\end{cases}, \tag{44}$$

$$\begin{cases}\boldsymbol{\tau}_4\dot{\mathbf{x}}_{4d} + \mathbf{x}_{4d} = \mathbf{x}_{4c} \\ \mathbf{x}_{4d}(0) = \mathbf{x}_{4c}(0)\end{cases}, \tag{45}$$

where $\boldsymbol{\tau}_3 = \mathrm{diag}(\tau_{31}, \tau_{32}, \tau_{33})$ and $\boldsymbol{\tau}_4 = \mathrm{diag}(\tau_{41}, \tau_{42}, \tau_{43})$ are the filter time constant diagonal matrixes.

The 3D reduced-order ESO used to estimate the lumped disturbance $\mathbf{d}_1$ can be formulated as:

$$\begin{cases}\dot{\mathbf{z}}_1 = -\boldsymbol{\beta}_1\mathbf{z}_1 - \boldsymbol{\beta}_1^2\mathbf{x}_1 - \boldsymbol{\beta}_1\left[\mathbf{F}_1 + \mathbf{G}_1\mathbf{x}_2^*\right] \\ \hat{\mathbf{d}}_1 = \mathbf{z}_1 + \boldsymbol{\beta}_1\mathbf{x}_1\end{cases}, \tag{46}$$

where $\mathbf{z}_1 = [z_{11}, z_{12}]^T$ denotes the auxiliary signal variable vector. $\boldsymbol{\beta}_1 = [\beta_{11}, \beta_{12}]^T$ is the observer gain diagonal matrix and $\beta_{1i} > 0$, which determines the initial estimated error value and error convergence rate.

Similarly, the estimates $\hat{\mathbf{d}}_2$, $\hat{\mathbf{d}}_3$, and $\hat{\mathbf{d}}_4$ can be constructed as:

$$\begin{cases}\dot{\mathbf{z}}_i = -\boldsymbol{\beta}_i\mathbf{z}_i - \boldsymbol{\beta}_i^2\mathbf{x}_i - \boldsymbol{\beta}_i\left[\mathbf{F}_i + \mathbf{G}_i\mathbf{x}_{i+1}\right] \\ \hat{\mathbf{d}}_i = \mathbf{z}_i + \boldsymbol{\beta}_i\mathbf{x}_i\end{cases}, \ i = 2, 3, 4, \tag{47}$$

where $\mathbf{z}_i = [z_{i1}, z_{i2}, z_{i3}]^T$ denote the auxiliary signal variable vectors. $\boldsymbol{\beta}_i = [\beta_{i1}, \beta_{i2}, \beta_{i3}]^T$ are the observer gain diagonal matrixes, and $\beta_{ij} > 0$ $(j = 1, 2, 3)$.

Finally, the proposed control law includes virtual control commands, which can be summarized as follows:

$$\begin{cases}\mathbf{s}_0 = \mathbf{x}_0 \\ \mathbf{x}_{1c} = -\mathbf{k}_0\mathbf{s}_0 \\ \boldsymbol{\tau}_1\dot{\mathbf{x}}_{1d} + \mathbf{x}_{1d} = \mathbf{x}_{1c}, \mathbf{x}_{1d}(0) = \mathbf{x}_{1c}(0) \\ \mathbf{s}_1 = \mathbf{x}_1 - \mathbf{x}_{1d} \\ \mathbf{x}_{2c}^* = \mathbf{G}_1^{-1}[-\mathbf{F}_1 - \hat{\mathbf{d}}_1 + \dot{\mathbf{x}}_{1d} - \mathbf{k}_1\mathbf{s}_1] \\ \boldsymbol{\tau}_2\dot{\mathbf{x}}_{2d}^* + \mathbf{x}_{2d}^* = \mathbf{x}_{2c}^*, \mathbf{x}_{2d}^*(0) = \mathbf{x}_{2c}^*(0) \\ \mathbf{x}_{2d} = [\mathbf{x}_{2d}^*, 0]^T \\ \mathbf{s}_2 = \mathbf{x}_2 - \mathbf{x}_{2d} \\ \mathbf{x}_{3c} = \mathbf{G}_2^{-1}[-\mathbf{F}_2 - \hat{\mathbf{d}}_2 + \dot{\mathbf{x}}_{2d} - \mathbf{k}_2\mathbf{s}_2] \\ \boldsymbol{\tau}_3\dot{\mathbf{x}}_{3d} + \mathbf{x}_{3d} = \mathbf{x}_{3c}, \mathbf{x}_{3d}(0) = \mathbf{x}_{3c}(0) \\ \mathbf{s}_3 = \mathbf{x}_3 - \mathbf{x}_{3d} \\ \mathbf{x}_{4c} = \mathbf{G}_3^{-1}[-\mathbf{F}_3 - \hat{\mathbf{d}}_3 + \dot{\mathbf{x}}_{3d} - \mathbf{k}_3\mathbf{s}_3] \\ \boldsymbol{\tau}_4\dot{\mathbf{x}}_{4d} + \mathbf{x}_{4d} = \mathbf{x}_{4c}, \mathbf{x}_{4d}(0) = \mathbf{x}_{4c}(0) \\ \mathbf{s}_4 = \mathbf{x}_4 - \mathbf{x}_{4d} \\ \mathbf{u} = \mathbf{G}_4^{-1}[-\mathbf{F}_4 - \hat{\mathbf{d}}_4 + \dot{\mathbf{x}}_{4d} - \mathbf{k}_4\mathbf{s}_4]\end{cases}. \tag{48}$$

4. Stability analysis

For the 3D nonlinear strict-feedback IGC model, Eqs. (26) and (27) and the proposed ACIGC scheme in Eq. (48), the stability of the closed-loop system is proved using Lyapunov theory.

Assumption 6. The estimation error $\left\|\mathbf{d}_i - \hat{\mathbf{d}}_i\right\| < m_i, \ i = 1, 2, 3, 4$ (m_i is a positive constant) can be guaranteed using the 3D reduced-order ESO estimation system-lumped disturbance $\mathbf{d}_i, \ i = 1, 2, 3, 4$. Furthermore, the observer estimation errors can converge to an arbitrarily small range by adjusting the observer gains [32].

Remark 3. The observer gains of the 3D reduced-order ESO determine the initial estimated error values and error convergence rates. By increasing the observer gains, the disturbance estimation errors can converge to an arbitrarily small range.

Theorem 1. *Based on the given Assumption 1–6, the proposed ACIGC law, Eq. (48), and the 3D reduced-order ESO for the proposed 3D strict-feedback nonlinear IGC model in Eqs. (26) and (27) with mismatched uncertainties, if κ is a constant, and the controller parameters $\mathbf{k}_i,\ i = 0, 1, \cdots, 4$, filter time constants $\boldsymbol{\tau}_j,\ j = 1, 2, 3, 4$ satisfy Eq. (72), all the states of the closed-loop system are uniformly ultimately bounded.*

The filter tracking errors can be defined as

$$\begin{cases} \mathbf{e}_1 = \mathbf{x}_{1d} - \mathbf{x}_{1c} \\ \mathbf{e}_2 = \mathbf{x}_{2d}^* - \mathbf{x}_{2c}^* \\ \mathbf{e}_3 = \mathbf{x}_{3d} - \mathbf{x}_{3c} \\ \mathbf{e}_4 = \mathbf{x}_{4d} - \mathbf{x}_{4c} \end{cases}. \tag{49}$$

Differentiating Eq. (49) gives

$$\begin{cases} \dot{\mathbf{e}}_1 = -\boldsymbol{\tau}_1^{-1}\mathbf{e}_1 - \dot{\mathbf{x}}_{1c} \\ \dot{\mathbf{e}}_2 = -\boldsymbol{\tau}_2^{-1}\mathbf{e}_2 - \dot{\mathbf{x}}_{2c}^* \\ \dot{\mathbf{e}}_3 = -\boldsymbol{\tau}_3^{-1}\mathbf{e}_3 - \dot{\mathbf{x}}_{3c} \\ \dot{\mathbf{e}}_4 = -\boldsymbol{\tau}_4^{-1}\mathbf{e}_4 - \dot{\mathbf{x}}_{4c} \end{cases}. \tag{50}$$

Equation (50) is calculated by simple algebra to obtain

$$\mathbf{e}_1^T\dot{\mathbf{e}}_1 = -\mathbf{e}_1^T\boldsymbol{\tau}_1^{-1}\mathbf{e}_1 - \mathbf{e}_1^T\dot{\mathbf{x}}_{1c} \le -\mathbf{e}_1^T\left(\boldsymbol{\tau}_1^{-1} - \frac{1}{2}\left\|\dot{\mathbf{x}}_{1c}\right\|^2\mathbf{I}_2\right)\mathbf{e}_1 + \frac{1}{2}, \tag{51}$$

$$\mathbf{e}_2^T\dot{\mathbf{e}}_2 = -\mathbf{e}_2^T\boldsymbol{\tau}_2^{-1}\mathbf{e}_2 - \mathbf{e}_2^T\dot{\mathbf{x}}_{2c} \le -\mathbf{e}_2^T\left(\boldsymbol{\tau}_2^{-1} - \frac{1}{2}\left\|\dot{\mathbf{x}}_{2c}^*\right\|^2\mathbf{I}_2\right)\mathbf{e}_2 + \frac{1}{2}, \tag{52}$$

$$\mathbf{e}_3^T\dot{\mathbf{e}}_3 = -\mathbf{e}_3^T\boldsymbol{\tau}_3^{-1}\mathbf{e}_3 - \mathbf{e}_3^T\dot{\mathbf{x}}_{3c} \le -\mathbf{e}_3^T\left(\boldsymbol{\tau}_3^{-1} - \frac{1}{2}\left\|\dot{\mathbf{x}}_{3c}\right\|^2\mathbf{I}_3\right)\mathbf{e}_3 + \frac{1}{2}, \tag{53}$$

$$\mathbf{e}_4^T\dot{\mathbf{e}}_4 = -\mathbf{e}_4^T\boldsymbol{\tau}_4^{-1}\mathbf{e}_4 - \mathbf{e}_4^T\dot{\mathbf{x}}_{4c} \le -\mathbf{e}_4^T\left(\boldsymbol{\tau}_4^{-1} - \frac{1}{2}\left\|\dot{\mathbf{x}}_{4c}\right\|^2\mathbf{I}_3\right)\mathbf{e}_4 + \frac{1}{2}, \tag{54}$$

where $\mathbf{I}_2$ and $\mathbf{I}_3$ denote identity matrix.

We let the Lyapunov function candidate be

$$V_s = V_0 + V_1 + V_2 + V_3 + V_4, \tag{55}$$

where

$$V_0 = \frac{1}{2}\mathbf{s}_0^T\mathbf{s}_0, \tag{56}$$

$$V_1 = \frac{1}{2}\mathbf{s}_1^T\mathbf{s}_1 + \frac{1}{2}\mathbf{e}_1^T\mathbf{e}_1, \tag{57}$$

$$V_2 = \frac{1}{2}\mathbf{s}_2^T\mathbf{s}_2 + \frac{1}{2}\mathbf{e}_2^T\mathbf{e}_2, \tag{58}$$

$$V_3 = \frac{1}{2}\mathbf{s}_3^T\mathbf{s}_3 + \frac{1}{2}\mathbf{e}_3^T\mathbf{e}_3, \tag{59}$$

$$V_4 = \frac{1}{2}\mathbf{s}_4^T\mathbf{s}_4 + \frac{1}{2}\mathbf{e}_4^T\mathbf{e}_4. \tag{60}$$

Combining Eqs. (48)–(50), after some algebraic computations, we have

$$\begin{aligned} \mathbf{s}_0^T\dot{\mathbf{s}}_0 &= \mathbf{s}_0^T\dot{\mathbf{x}}_0 = \mathbf{s}_0^T\mathbf{x}_1 \\ &= \mathbf{s}_0^T\left(\mathbf{s}_1 + \mathbf{e}_1 + \mathbf{x}_{1c}\right) \\ &= \mathbf{s}_0^T\left(\mathbf{s}_1 + \mathbf{e}_1 - \mathbf{k}_0\mathbf{s}_0\right) \\ &\le -\mathbf{s}_0^T\left[\mathbf{k}_0 - \frac{1}{2}\mathbf{I}_2\right]\mathbf{s}_0 + \mathbf{s}_1^T\mathbf{s}_1 + \mathbf{e}_1^T\mathbf{e}_1 \end{aligned}, \tag{61}$$

$$\begin{aligned} \mathbf{s}_1^T\dot{\mathbf{s}}_1 &= \mathbf{s}_1^T\left(\dot{\mathbf{x}}_1 - \dot{\mathbf{x}}_{1d}\right) = \mathbf{s}_1^T\left(\mathbf{F}_1 + \mathbf{G}_1\mathbf{x}_2^* + \mathbf{d}_1 - \dot{\mathbf{x}}_{1d}\right) \\ &= \mathbf{s}_1^T\left[\mathbf{F}_1 + \mathbf{G}_1\left(\mathbf{s}_2^* + \mathbf{e}_2 + \mathbf{x}_{2c}^*\right) + \mathbf{d}_1 - \dot{\mathbf{x}}_{1d}\right] \\ &= \mathbf{s}_1^T\mathbf{G}_1\left(\mathbf{s}_2^* + \mathbf{e}_2\right) + \mathbf{s}_1^T\left(\mathbf{d}_1 - \hat{\mathbf{d}}_1\right) - \mathbf{s}_1^T\mathbf{k}_1\mathbf{s}_1 \\ &\le -\mathbf{s}_1^T\left[\mathbf{k}_1 - \frac{1}{2}\mathbf{G}_1^2 - \frac{1}{4}\mathbf{I}_2\right]\mathbf{s}_1 + \mathbf{s}_2^T\mathbf{s}_2 + \mathbf{e}_2^T\mathbf{e}_2 + m_1^2 \end{aligned}, \tag{62}$$

$$\begin{aligned} \mathbf{s}_2^T\dot{\mathbf{s}}_2 &= \mathbf{s}_2^T\left(\dot{\mathbf{x}}_2 - \dot{\mathbf{x}}_{2d}\right) = \mathbf{s}_2^T\left(\mathbf{F}_2 + \mathbf{G}_2\mathbf{x}_3 + \mathbf{d}_2 - \dot{\mathbf{x}}_{2d}\right) \\ &= \mathbf{s}_2^T\left[\mathbf{F}_2 + \mathbf{G}_2\left(\mathbf{s}_3 + \mathbf{e}_3 + \mathbf{x}_{3c}\right) + \mathbf{d}_2 - \dot{\mathbf{x}}_{2d}\right] \\ &= \mathbf{s}_2^T\mathbf{G}_2\left(\mathbf{s}_3 + \mathbf{e}_3\right) + \mathbf{s}_2^T\left(\mathbf{d}_2 - \hat{\mathbf{d}}_2\right) - \mathbf{s}_2^T\mathbf{k}_2\mathbf{s}_2 \\ &\le -\mathbf{s}_2^T\left[\mathbf{k}_2 - \frac{1}{2}\mathbf{G}_2^2 - \frac{1}{4}\mathbf{I}_3\right]\mathbf{s}_2 + \mathbf{s}_3^T\mathbf{s}_3 + \mathbf{e}_3^T\mathbf{e}_3 + m_2^2 \end{aligned}, \tag{63}$$

$$\begin{aligned}\mathbf{s}_3^T\dot{\mathbf{s}}_3 &= \mathbf{s}_3^T\left(\dot{\mathbf{x}}_3-\dot{\mathbf{x}}_{3d}\right)=\mathbf{s}_3^T\left(\mathbf{F}_3+\mathbf{G}_3\mathbf{x}_4+\mathbf{d}_3-\dot{\mathbf{x}}_{3d}\right)\\ &= \mathbf{s}_3^T\left[\mathbf{F}_3+\mathbf{G}_3\left(\mathbf{s}_4+\mathbf{e}_4+\mathbf{x}_{4c}\right)+\mathbf{d}_3-\dot{\mathbf{x}}_{3d}\right]\\ &= \mathbf{s}_3^T\mathbf{G}_3\left(\mathbf{s}_4+\mathbf{e}_4\right)+\mathbf{s}_3^T\left(\mathbf{d}_3-\hat{\mathbf{d}}_3\right)-\mathbf{s}_3^T\mathbf{k}_3\mathbf{s}_3\\ &\le -\mathbf{s}_3^T\left[\mathbf{k}_3-\frac{1}{2}\mathbf{G}_3^2-\frac{1}{4}\mathbf{I}_3\right]\mathbf{s}_3+\mathbf{s}_4^T\mathbf{s}_4+\mathbf{e}_4^T\mathbf{e}_4+m_3^2\end{aligned}, \tag{64}$$

$$\begin{aligned}\mathbf{s}_4^T\dot{\mathbf{s}}_4 &= \mathbf{s}_4^T\left(\dot{\mathbf{x}}_4-\dot{\mathbf{x}}_{4d}\right)=\mathbf{s}_4^T\left(\mathbf{F}_4+\mathbf{G}_4\mathbf{u}+\mathbf{d}_4-\dot{\mathbf{x}}_{4d}\right)\\ &= \mathbf{s}_4^T\left[\mathbf{d}_4-\hat{\mathbf{d}}_4-\mathbf{k}_4\mathbf{s}_4\right]\\ &\le -\mathbf{s}_4^T\left[\mathbf{k}_4-\frac{1}{4}\mathbf{I}_3\right]\mathbf{s}_4+m_4^2\end{aligned}. \tag{65}$$

Differentiating Eqs. (56)–(60) and combining Eqs. (51)–(54) and (61)–(65) yields

$$\dot{V}_0=\mathbf{s}_0^T\dot{\mathbf{s}}_0\le -\mathbf{s}_0^T\left[\mathbf{k}_0-\frac{1}{2}\mathbf{I}_2\right]\mathbf{s}_0+\mathbf{s}_1^T\mathbf{s}_1+\mathbf{e}_1^T\mathbf{e}_1, \tag{66}$$

$$\begin{aligned}\dot{V}_1 &= \mathbf{s}_1^T\dot{\mathbf{s}}_1+\mathbf{e}_1^T\dot{\mathbf{e}}_1\\ &\le -\mathbf{s}_1^T\left[\mathbf{k}_1-\frac{1}{2}\mathbf{G}_1^2-\frac{1}{4}\mathbf{I}_2\right]\mathbf{s}_1+\mathbf{s}_2^T\mathbf{s}_2+\mathbf{e}_2^T\mathbf{e}_2+m_1^2-\mathbf{e}_1^T\left(\boldsymbol{\tau}_1^{-1}-\frac{1}{2}\left\|\dot{\mathbf{x}}_{1c}\right\|^2\mathbf{I}_2\right)\mathbf{e}_1+\frac{1}{2}\end{aligned}, \tag{67}$$

$$\begin{aligned}\dot{V}_2 &= \mathbf{s}_2^T\dot{\mathbf{s}}_2+\mathbf{e}_2^T\dot{\mathbf{e}}_2\\ &\le -\mathbf{s}_2^T\left[\mathbf{k}_2-\frac{1}{2}\mathbf{G}_2^2-\frac{1}{4}\mathbf{I}_3\right]\mathbf{s}_2+\mathbf{s}_3^T\mathbf{s}_3+\mathbf{e}_3^T\mathbf{e}_3+m_2^2-\mathbf{e}_2^T\left(\boldsymbol{\tau}_2^{-1}-\frac{1}{2}\left\|\dot{\mathbf{x}}_{2c}^*\right\|^2\mathbf{I}_2\right)\mathbf{e}_2+\frac{1}{2}\end{aligned}, \tag{68}$$

$$\begin{aligned}\dot{V}_3 &= \mathbf{s}_3^T\dot{\mathbf{s}}_3+\mathbf{e}_3^T\dot{\mathbf{e}}_3\\ &\le -\mathbf{s}_3^T\left[\mathbf{k}_3-\frac{1}{2}\mathbf{G}_3^2-\frac{1}{4}\mathbf{I}_3\right]\mathbf{s}_3+\mathbf{s}_4^T\mathbf{s}_4+\mathbf{e}_4^T\mathbf{e}_4+m_3^2-\mathbf{e}_3^T\left(\boldsymbol{\tau}_3^{-1}-\frac{1}{2}\left\|\dot{\mathbf{x}}_{3c}\right\|^2\mathbf{I}_3\right)\mathbf{e}_3+\frac{1}{2}\end{aligned}, \tag{69}$$

$$\begin{aligned}\dot{V}_4 &= \mathbf{s}_4^T\dot{\mathbf{s}}_4+\mathbf{e}_4^T\dot{\mathbf{e}}_4\\ &\le -\mathbf{s}_4^T\left[\mathbf{k}_4-\frac{1}{4}\mathbf{I}_3\right]\mathbf{s}_4+m_4^2-\mathbf{e}_4^T\left(\boldsymbol{\tau}_4^{-1}-\frac{1}{2}\left\|\dot{\mathbf{x}}_{4c}\right\|^2\mathbf{I}_3\right)\mathbf{e}_4+\frac{1}{2}\end{aligned}. \tag{70}$$

Differentiating Eq. (55), and combining Eqs. (66)–(70) yields

$$\begin{aligned}\dot{V}_s =\ & \dot{V}_0+\dot{V}_1+\dot{V}_2+\dot{V}_3+\dot{V}_4\\ \le\ & -\mathbf{s}_0^T\left[\mathbf{k}_0-\frac{1}{2}\mathbf{I}_2\right]\mathbf{s}_0-\mathbf{s}_1^T\left[\mathbf{k}_1-\frac{1}{2}\mathbf{G}_1^2-\frac{5}{4}\mathbf{I}_2\right]\mathbf{s}_1-\mathbf{s}_2^T\left[\mathbf{k}_2-\frac{1}{2}\mathbf{G}_2^2-\frac{5}{4}\mathbf{I}_3\right]\mathbf{s}_2\\ & -\mathbf{s}_3^T\left[\mathbf{k}_3-\frac{1}{2}\mathbf{G}_3^2-\frac{5}{4}\mathbf{I}_3\right]\mathbf{s}_3-\mathbf{s}_4^T\left[\mathbf{k}_4-\frac{5}{4}\mathbf{I}_3\right]\mathbf{s}_4-\mathbf{e}_1^T\left(\boldsymbol{\tau}_1^{-1}-\frac{1}{2}\left\|\dot{\mathbf{x}}_{1c}\right\|^2\mathbf{I}_2-\mathbf{I}_2\right)\mathbf{e}_1\\ & -\mathbf{e}_2^T\left(\boldsymbol{\tau}_2^{-1}-\frac{1}{2}\left\|\dot{\mathbf{x}}_{2c}^*\right\|^2\mathbf{I}_2-\mathbf{I}_2\right)\mathbf{e}_2-\mathbf{e}_3^T\left(\boldsymbol{\tau}_3^{-1}-\frac{1}{2}\left\|\dot{\mathbf{x}}_{3c}\right\|^2\mathbf{I}_3-\mathbf{I}_3\right)\mathbf{e}_3\\ & -\mathbf{e}_4^T\left(\boldsymbol{\tau}_4^{-1}-\frac{1}{2}\left\|\dot{\mathbf{x}}_{4c}\right\|^2\mathbf{I}_3-\mathbf{I}_3\right)\mathbf{e}_4+m_1^2+m_2^2+m_3^2+m_4^2+2\end{aligned}. \tag{71}$$

The appropriate control law parameters and filter parameters are selected, such that

$$\begin{cases}\mathbf{k}_0-\frac{1}{2}\mathbf{I}_2\ge\frac{1}{2}\kappa\mathbf{I}_2\\ \mathbf{k}_1-\frac{1}{2}\mathbf{G}_1^2-\frac{5}{4}\mathbf{I}_2\ge\frac{1}{2}\kappa\mathbf{I}_2\\ \mathbf{k}_2-\frac{1}{2}\mathbf{G}_2^2-\frac{5}{4}\mathbf{I}_3\ge\frac{1}{2}\kappa\mathbf{I}_3\\ \mathbf{k}_3-\frac{1}{2}\mathbf{G}_3^2-\frac{5}{4}\mathbf{I}_3\ge\frac{1}{2}\kappa\mathbf{I}_3\\ \mathbf{k}_4-\frac{5}{4}\mathbf{I}_3\ge\frac{1}{2}\kappa\mathbf{I}_3\\ \boldsymbol{\tau}_1^{-1}-\frac{1}{2}\left\|\dot{\mathbf{x}}_{1c}\right\|^2\mathbf{I}_2-\mathbf{I}_2\ge\frac{1}{2}\kappa\mathbf{I}_2\\ \boldsymbol{\tau}_2^{-1}-\frac{1}{2}\left\|\dot{\mathbf{x}}_{2c}^*\right\|^2\mathbf{I}_2-\mathbf{I}_2\ge\frac{1}{2}\kappa\mathbf{I}_2\\ \boldsymbol{\tau}_3^{-1}-\frac{1}{2}\left\|\dot{\mathbf{x}}_{3c}\right\|^2\mathbf{I}_3-\mathbf{I}_3\ge\frac{1}{2}\kappa\mathbf{I}_3\\ \boldsymbol{\tau}_4^{-1}-\frac{1}{2}\left\|\dot{\mathbf{x}}_{4c}\right\|^2\mathbf{I}_3-\mathbf{I}_3\ge\frac{1}{2}\kappa\mathbf{I}_3\end{cases}. \tag{72}$$

We define $\eta=m_1^2+m_2^2+m_3^2+m_4^2+2$; therefore, Eq. (72) can be rewritten as

$$\dot{V}_s\le -\kappa V_s+\eta. \tag{73}$$

Table 1
Missile-related parameters.

Name	Value	Name	Value	Name	Value
m	1,200 kg	c_y^{β}	−0.081	m_y^{β}	−27.30
S	0.43 m^2	$c_y^{\delta_z}$	5.75	$m_y^{\delta_y}$	−26.60
L	0.69 m	c_z^{α}	0.091	m_z^{α}	−28.15
J_x	100 kg·m^2	c_z^{β}	−56.32	$m_z^{\delta_z}$	−27.90
J_y	5,800 kg·m^2	$c_z^{\delta_y}$	−5.6	τ_x	0.1
J_z	5,700 kg·m^2	m_x^{α}	0.45	τ_y	0.1
ρ	1.1558 kg/m^3	m_x^{β}	−0.38	τ_z	0.1
c_y^{α}	57.15	$m_x^{\delta_x}$	2.13		

According to Eq. (73), we can obtain [33]

$$0 \le V_s(t) \le \left(V_s(0) - \frac{\eta}{\kappa}\right) e^{-\kappa t} + \frac{\eta}{\kappa}. \tag{74}$$

It is evident from Eq. (74) that V_s is bounded. Therefore, $\mathbf{s}_0$, $\mathbf{s}_1$, $\mathbf{s}_2$, $\mathbf{s}_3$, $\mathbf{s}_4$, $\mathbf{e}_1$, $\mathbf{e}_2$, $\mathbf{e}_3$, $\mathbf{e}_4$ are all uniformly ultimately bounded. And the system state vectors $\mathbf{x}_0$, $\mathbf{x}_1$, $\mathbf{x}_2$, $\mathbf{x}_3$, $\mathbf{x}_4$ are also uniformly ultimately bounded. Moreover, the above vectors can converge to a very small range by adjusting κ. That is to say, the vector $\mathbf{x}_0$ can be arbitrarily small, thus guaranteeing R for nominal range-to-go R_d tracking and q_2 for desired azimuth q_{2d} tracking.

Remark 4. For the proposed IGC and ACIGC schemes, the system states are ultimately uniformly bounded. It can also ensure that the missile-target distance R of all the missiles can accurately track the nominal range-to-go R_d until they hit the target to achieve a simultaneous attack at a predefined impact time T_d. The terminal-impact azimuth q_{2f} can also converge to a predefined impact azimuth q_{2d}. Thus, multiple missiles can simultaneously attack the targets at different azimuths.

Hereto, **Theorem 1** is proved.

5. Simulations

To verify the effectiveness and robustness of the proposed ACIGC scheme, six-degrees-of-freedom (6DOF) numerical simulations were performed.

Assuming that the STT missiles engaged in the attack are of the same type, the missile body parameters and aerodynamic coefficients are listed in Table 1. It should be noted that the aerodynamic forces from Eq. (17), can be approximated.

The uncertainties in Eqs. (17) and (18) can be formulated as follows

$$\begin{gathered}\begin{bmatrix} d_Y \\ d_Z \end{bmatrix} = \frac{1}{2}\begin{bmatrix} 100\sin(\pi t) + 16|\alpha| + 15|\beta| + 20|\alpha\beta| \\ 10\sin(2\pi t) + 10|\alpha\beta| \end{bmatrix} (N) \\ \begin{bmatrix} d_{M_x} \\ d_{M_y} \\ d_{M_z} \end{bmatrix} = \frac{1}{2}\begin{bmatrix} 0.1\alpha^3 + 0.1\beta^3 + 100\sin(0.5\pi t) \\ 0.2\alpha^3 + 0.2\beta^3 + 6000\sin(0.5\pi t) \\ 0.1\alpha^3 + 0.1\beta^3 + 5000\sin(0.5\pi t) \end{bmatrix} (\mathrm{N} \bullet \mathrm{m})\end{gathered} \tag{75}$$

The parameters of the proposed ACIGC scheme are selected as follows:

$$\mathbf{k}_0 = \mathrm{diag}(1.8, 1.5), \quad \mathbf{k}_1 = \mathrm{diag}(35, 36), \quad \mathbf{k}_2 = \mathrm{diag}(20, 18, 18), \quad \mathbf{k}_3 = \mathrm{diag}(10, 12, 11), \quad \text{and} \quad \mathbf{k}_4 = \mathrm{diag}(8, 12, 12).$$

The time constants of the filter are selected as

$$\boldsymbol{\tau}_1 = \mathrm{diag}(0.01, 0.01), \quad \boldsymbol{\tau}_2 = \mathrm{diag}(0.001, 0.001), \quad \boldsymbol{\tau}_3 = \mathrm{diag}(0.001, 0.001, 0.001), \quad \text{and} \quad \boldsymbol{\tau}_4 = \mathrm{diag}(0.001, 0.001, 0.001).$$

The 3D reduced-order ESO gain coefficients are selected as

$$\boldsymbol{\beta}_1 = \mathrm{diag}(10, 10), \quad \boldsymbol{\beta}_2 = \mathrm{diag}(15, 25, 25), \quad \boldsymbol{\beta}_3 = \mathrm{diag}(10, 20, 20), \quad \text{and} \quad \boldsymbol{\beta}_4 = \mathrm{diag}(10, 20, 20).$$

The center-of-mass motion models of the missile and target are expressed in Eq. (76). The guidance states R, q_1, and q_2 were calculated using Eq. (77).

$$\begin{cases} \dot{x} = V\cos\theta\cos\psi_V \\ \dot{y} = V\sin\theta \\ \dot{z} = -V\cos\theta\sin\psi_V \end{cases} \tag{76}$$

$$\begin{cases} R = \sqrt{(x_t - x_m)^2 + (y_t - y_m)^2 + (z_t - z_m)^2} \\ q_1 = \arctan\left((y_t - y_m)/\sqrt{(x_t - x_m)^2 + (z_t - z_m)^2}\right) \\ q_2 = -\arctan\left((z_t - z_m)/(x_t - x_m)\right) \end{cases} \tag{77}$$

The three missiles were assumed to be located at a certain distance from each other at the same height, with the same flight path and heading angles as those in the terminal guidance phase. The initial conditions of the missiles and the desired impact azimuths are listed in Table 2. Because the velocity of a hypersonic missile is significantly greater than that of a ground-moving target, a cooperative strategy

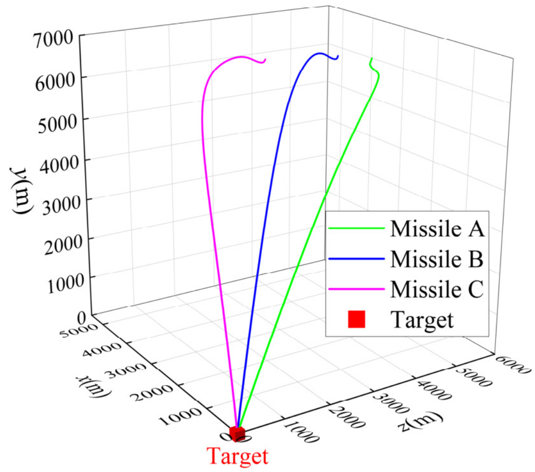

Fig. 3. Trajectories of the three missiles in Case 1. (For interpretation of the colors in the figure(s), the reader is referred to the web version of this article.)

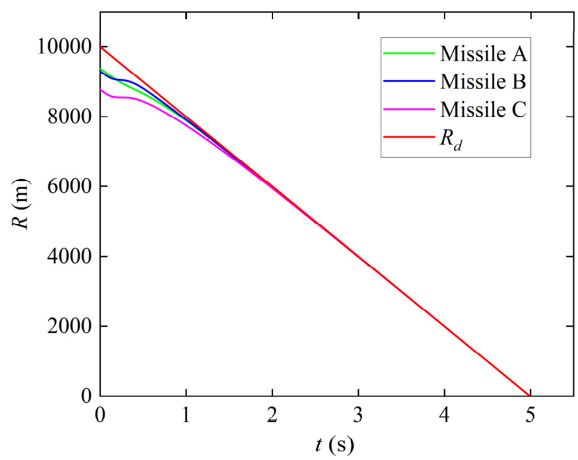

Fig. 4. The three missile-target distance variation curves and nominal ranges follow those of case 1.

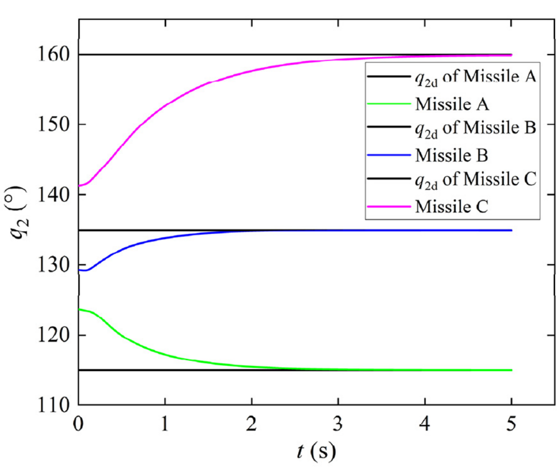

Fig. 5. Azimuth curves of the three missiles under Case 1.

Table 2
Initial conditions for the three missiles.

	(x_{m0}, y_{m0}, z_{m0}) (km)	V_M (m/s)	θ_{M0} (°)	ψ_{VM0} (°)	q_{2d}(°)
Missile A	(4.0,6.0,6.0)	2,000	−10	135	115
Missile B	(4.5,6.0,5.5)	2,000	−10	135	135
Missile C	(5.0,6.0,4.0)	2,000	−10	135	160

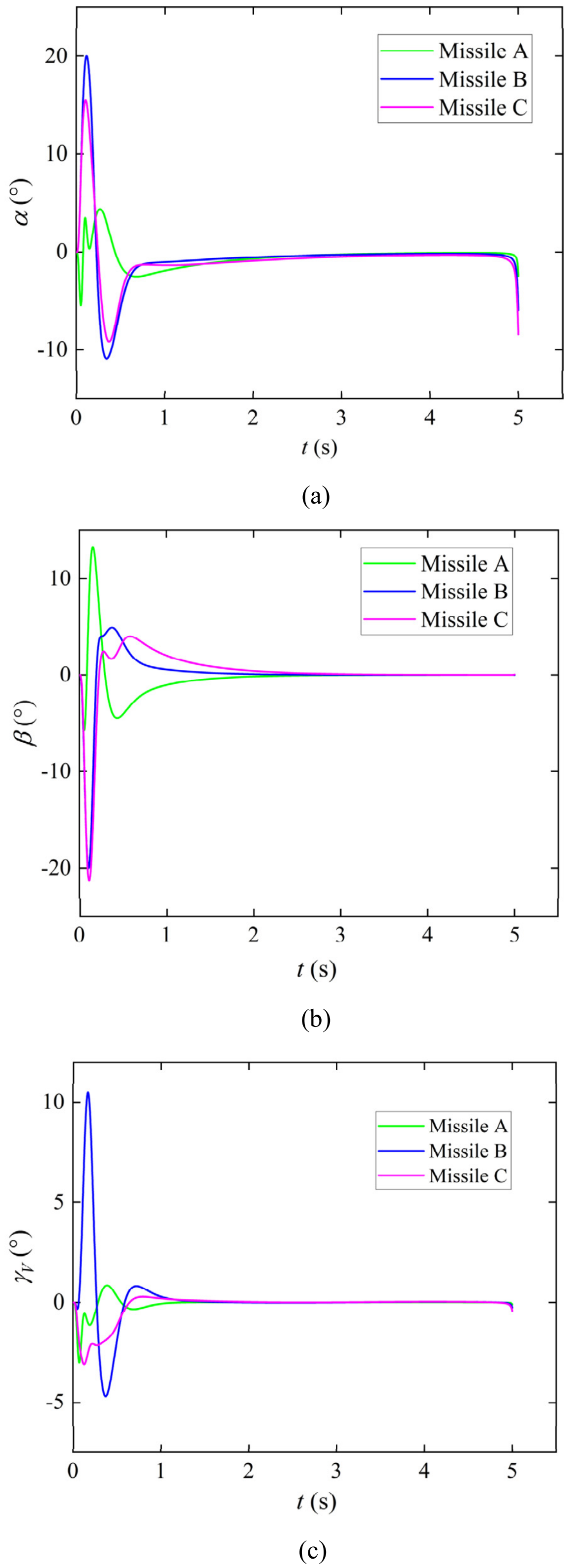

Fig. 6. Curves of α, β, and γ_V for three missiles in Case 1.

coefficient can be designed by treating the target as stationary. The desired impact time is set to $T_d = 5$ s. The cooperative strategy coefficient is set to $\gamma = 1.0$, based on the maximum initial missile-target distance.

A seeker has a dead zone when it is sufficiently close to the target. The guidance control system cannot operate correctly at this point because it fails to detect the relative motion of the missile-target. Therefore, it can be assumed that the rudder angles did not change. This simulation assumed that the dead-zone radius of the seeker was 30 m. The maximum rudder angle is $\delta_x^{\max} = \delta_y^{\max} = \delta_z^{\max} = 30°$.

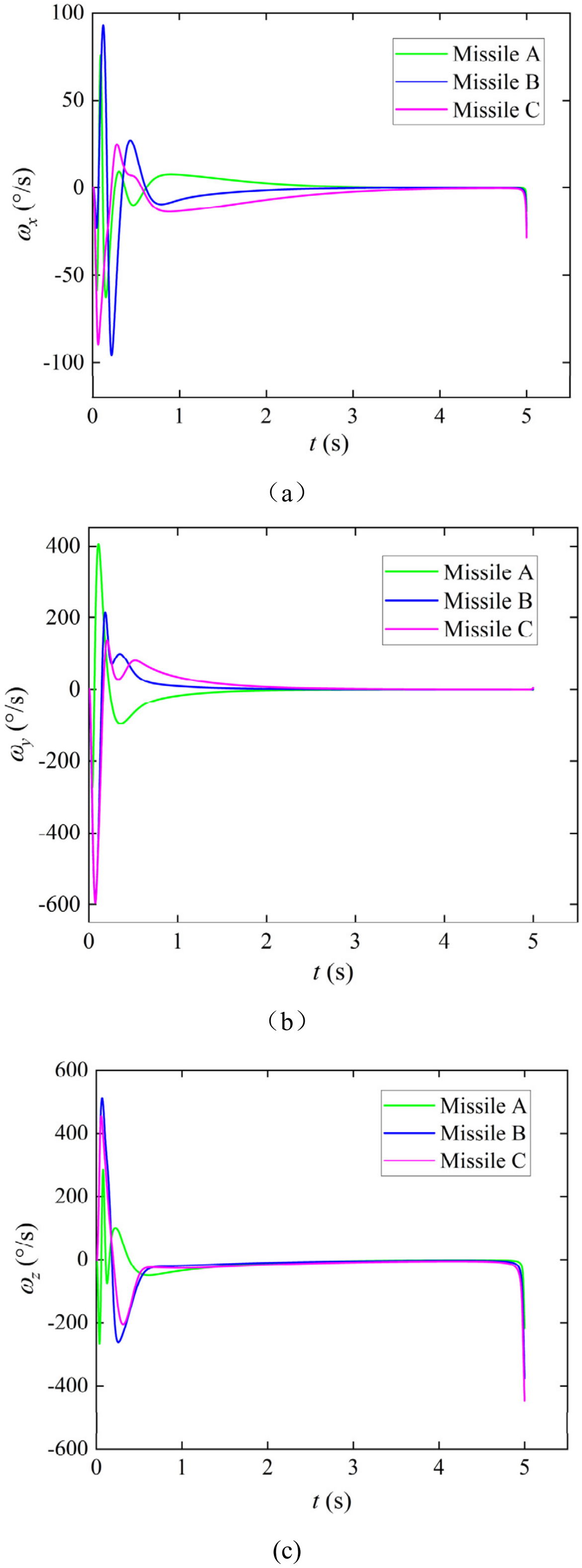

Fig. 7. Curves of angular rates ω_x, ω_y, and ω_z of three missiles in Case 1.

Case 1 *Ground fixed target*

The effectiveness of the proposed ACIGC scheme was verified by simultaneously attacking a stationary ground target using three missiles. The initial position of the target is determined using $(x_{t0}, y_{t0}, z_{t0}) = (0, 0, 0)$. Suppose that the coefficients of both aerodynamic forces and moments are reduced by 20% of their respective nominal values. The simulation results are summarized in Table 3 and Figs. 3–13.

As shown in Fig. 3 and Table 3, all three missiles could accurately attack a stationary ground target with miss distances of less than 1 m, errors of 1 ms between the actual impact time and predefined impact time, and errors of the terminal-impact azimuth of less than

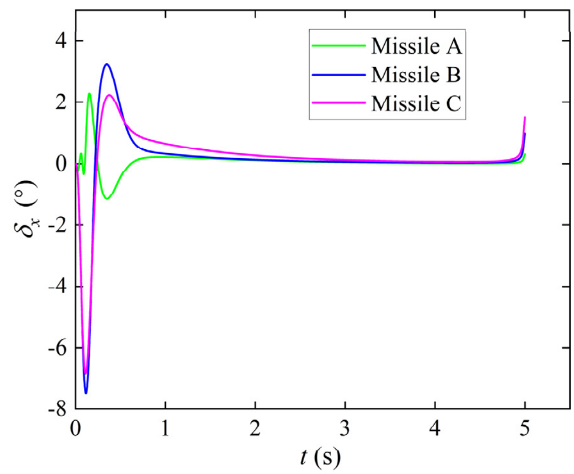

(a)

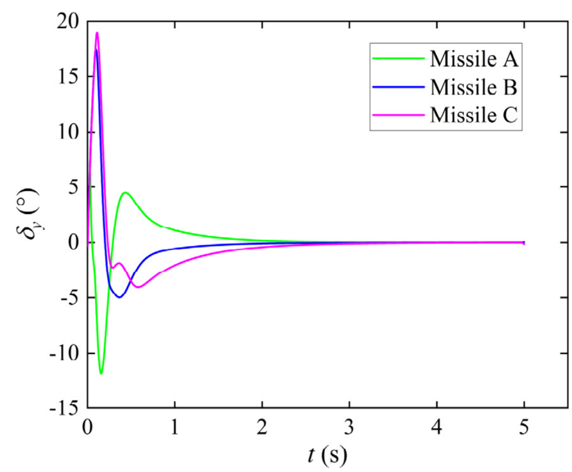

(b)

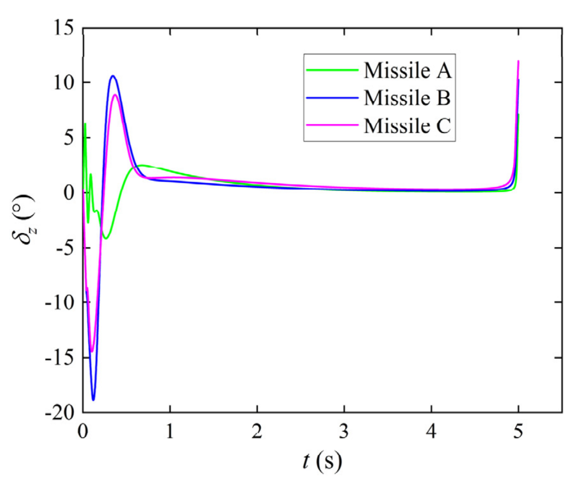

(c)

Fig. 8. Curves of rudder angles δ_x, δ_y, and δ_z for three missiles in Case 1.

Table 3
Simulation results for Case 1.

	T_d (s)	Impact time t_f (s)	q_{2d} (°)	q_{2f} (°)	Miss distance (m)
Missile A	5	4.999	115	114.97	0.2109
Missile B	5	4.999	135	134.97	0.4509
Missile C	5	4.999	160	159.95	0.8836

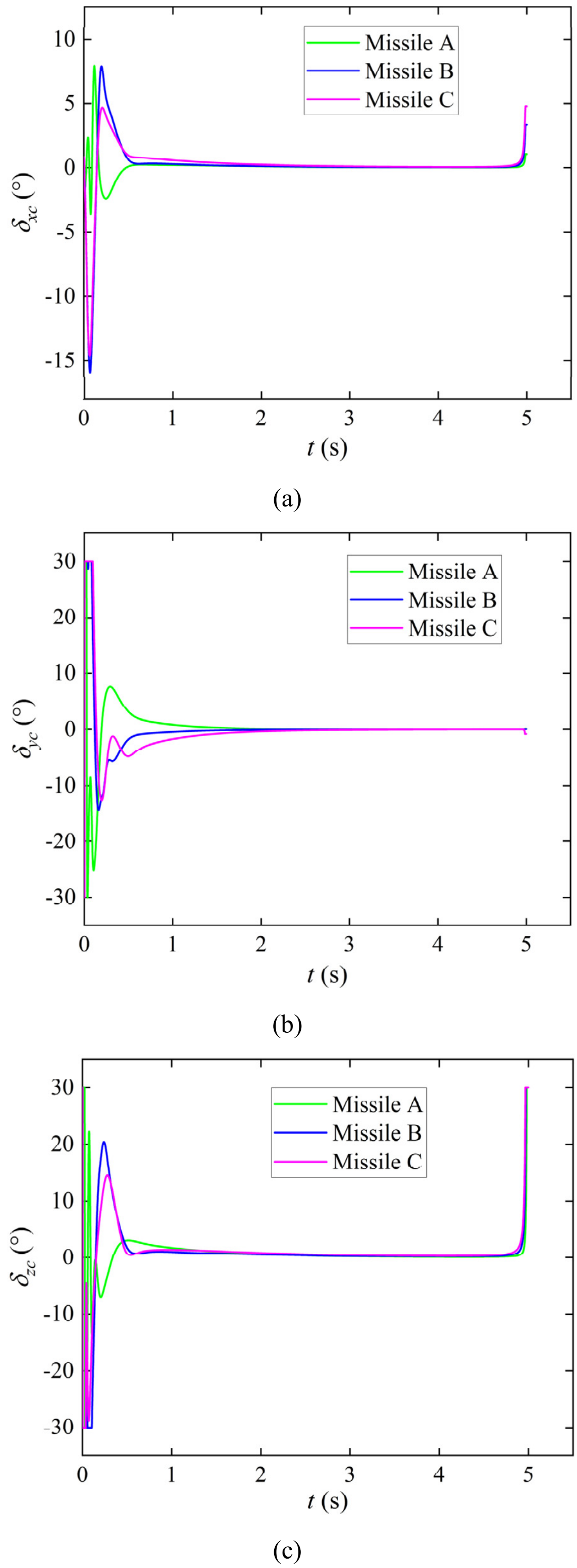

Fig. 9. Curves of control inputs δ_{xc}, δ_{yc}, and δ_{zc} for three missiles in Case 1.

1°. This confirms the effectiveness of the proposed scheme in the presence of system-lumped disturbances. Fig. 4 shows that the missile-target distance of the three missiles can quickly converge to the nominal missile-target range-to-go and subsequently track it until they hit the target. The errors between the actual and predefined impact times satisfy the design requirements. This indicates that the cooperative strategy for transforming the predefined impact time into the desired range using Eq. (28) is effective. Fig. 5 shows that the azimuths of the three missiles converge to the desired azimuths, confirming that the designed ACIGC scheme can satisfy the desired impact azimuth.

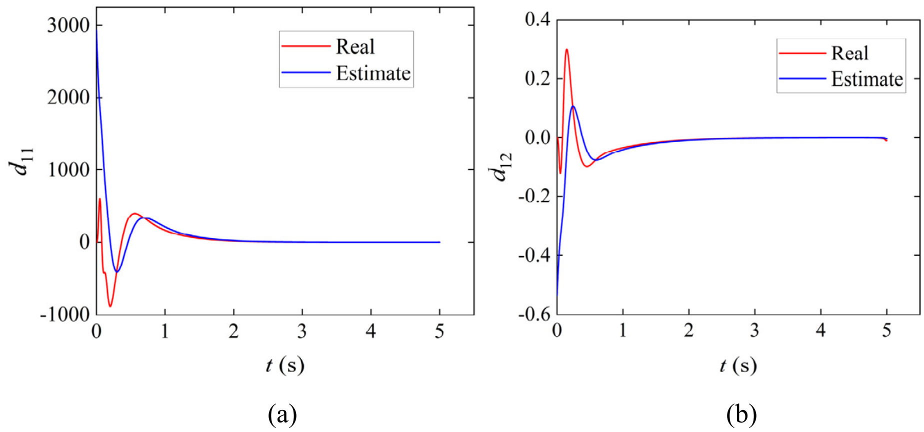

Fig. 10. Curves of $\mathbf{d}_1$ and its estimate for Missile A under Case 1.

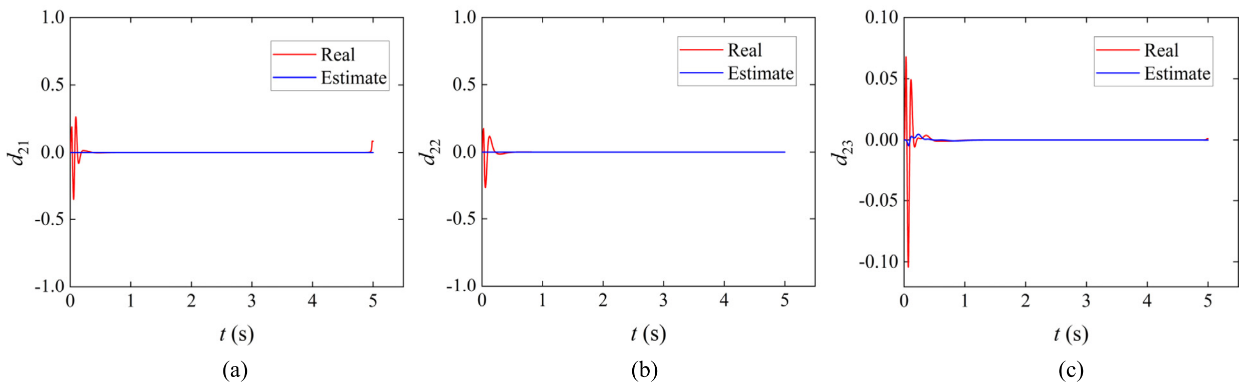

Fig. 11. Curves of $\mathbf{d}_2$ and its estimate for Missile A under Case 1.

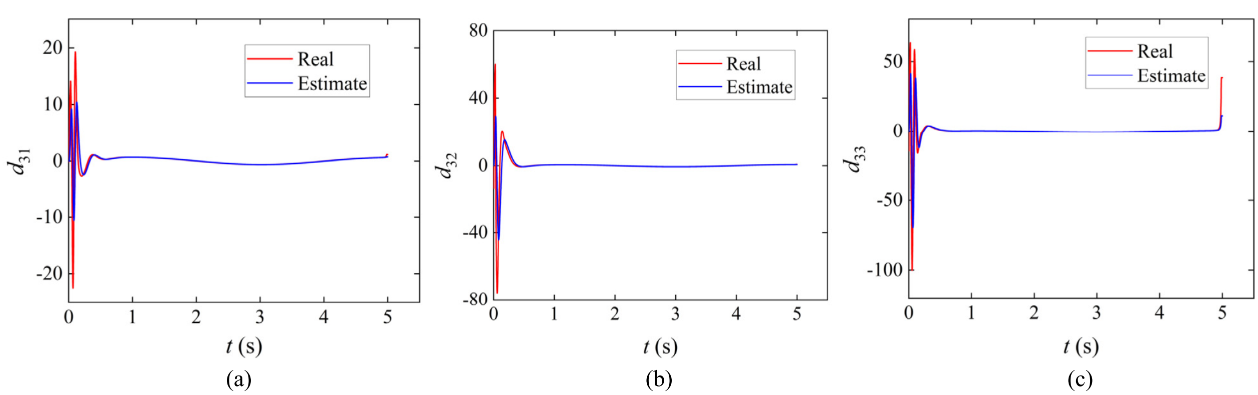

Fig. 12. Curves of $\mathbf{d}_3$ and its estimate for Missile A under Case 1.

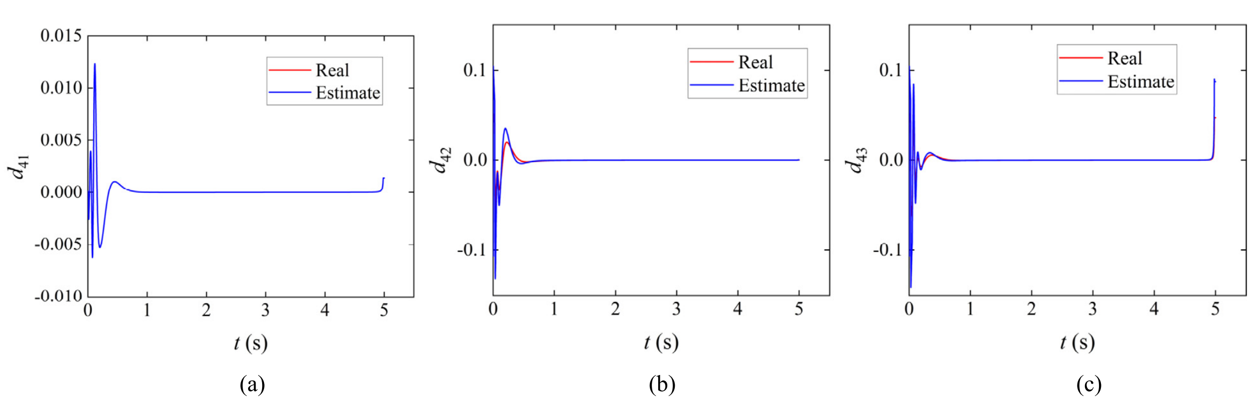

Fig. 13. Curves of $\mathbf{d}_4$ and its estimate for Missile A under Case 1.

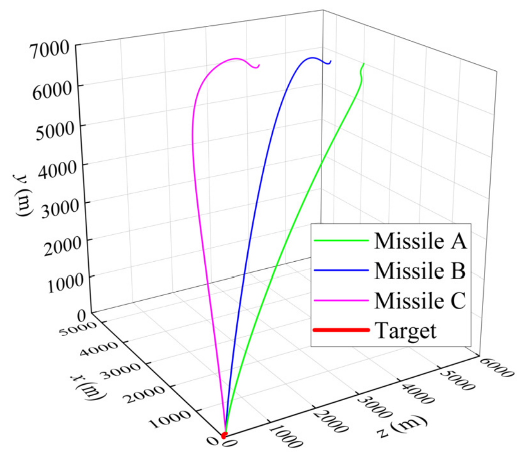

Fig. 14. Trajectories of the target and three missiles in Case 2.

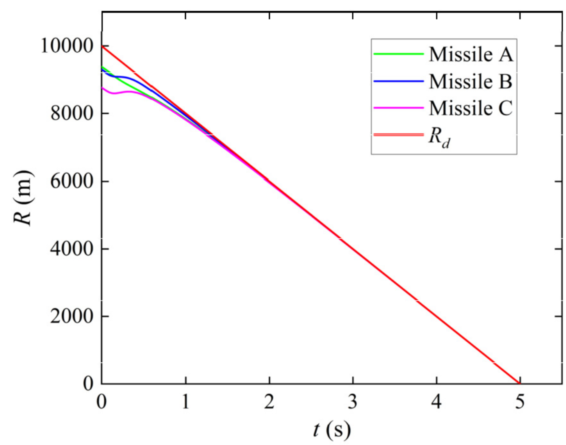

Fig. 15. The three missile-target distance variation curves and nominal ranges follow those in Case 2.

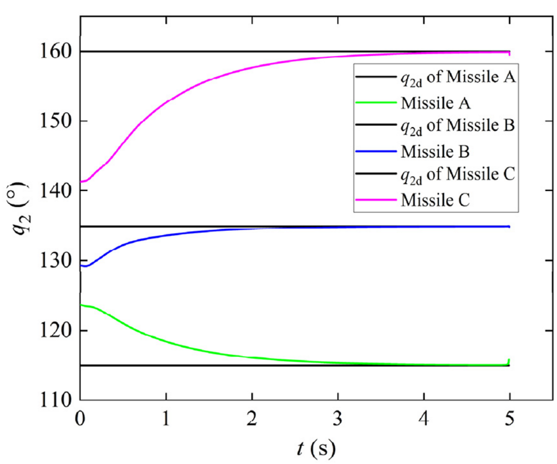

Fig. 16. Azimuth curves of the three missiles under Case 2.

The proposed ACIGC scheme assumes a small velocity-deflection angle. In other words, when the velocity-deflection angle is not zero, the errors caused by the approximation can be regarded as unmodeled parts of the system. Fig. 6 (c) shows that the velocity-deflection angles of the three missiles oscillate temporarily at the beginning, converge quickly to near zero, and remain there. This indicates that the missiles can still hit the target accurately when the velocity-deflection angle deviates from zero, further demonstrating that the proposed ACIGC scheme is effective despite uncertainties. As shown in Figs. 6 (b) and (c), the angle-of-attack and sideslip angle of the three missiles initially show short-term oscillations because the missiles need to adjust their attitudes to meet the desired missile-target distances and azimuths.

It can be observed from Fig. 7 that the three angular rates also oscillate briefly at the beginning to satisfy the initial attitude adjustments of the missiles and then remain stable. Fig. 8 shows that the rudder angles of the three missiles did not exceed the maximum rudder angle. Fig. 9 shows that although the three missiles initially show saturation inputs in both the pitch and yaw channels, the

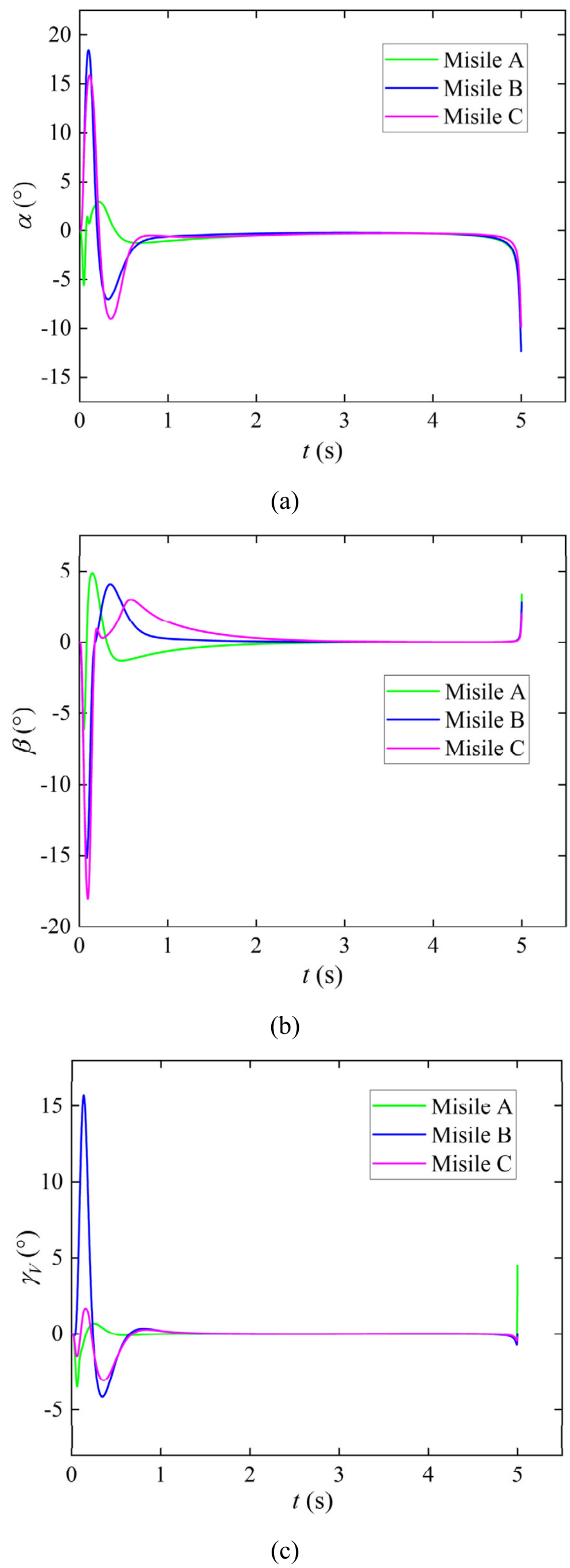

Fig. 17. Curves of α, β, and γ_V for three missiles in Case 2.

duration is short and there is still a design margin. Figs. 10–13 present system lumped disturbances and their estimated values by the reduced-order ESO, and it can be observed that the estimated values converge quickly to true values and track them until the target is hit.

Case 2 *Ground-maneuver target*

The effectiveness of the proposed ACIGC scheme was verified by simultaneously attacking a ground-maneuvering target using three missiles. The velocity of the ground target is $V_T = 30$ m/s, and the initial velocity-deflection angle is $\psi_{VT0} = 0°$. The target performs a

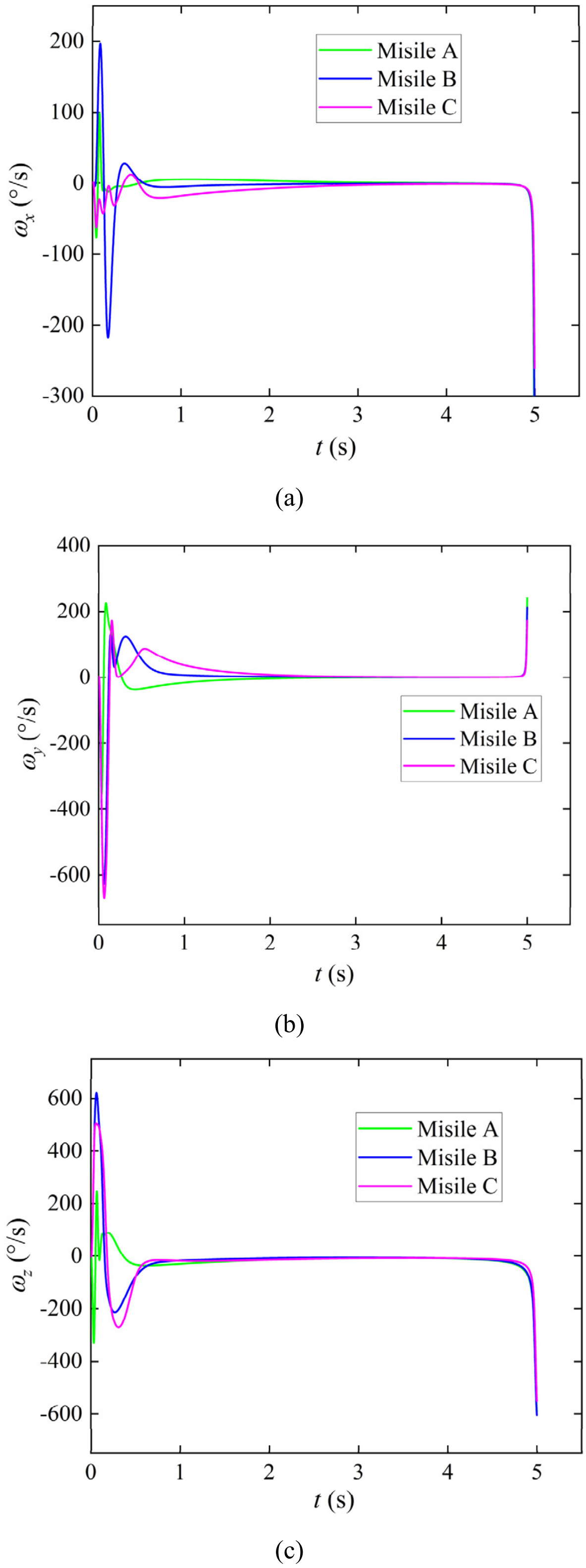

Fig. 18. Curves of angular rates ω_x, ω_y, and ω_z for three missiles in Case 2.

sinusoidal maneuver with a normal acceleration of $a_{tz} = 10 * \sin(\pi t) m/s^2$. Suppose that the coefficients of both aerodynamic forces and moments increase by 20% of their respective nominal values.

As shown in Table 4 and Figs. 14–16, all three missiles attacked the ground-maneuvered target accurately. The miss distance was < 1 m. The errors between the actual impact time and the predefined impact time were both 1 ms. The errors between the terminal-impact azimuth and desired impact azimuth were all less than 1°. For the ground-maneuvering target, Fig. 15 shows that the three missile-target distances can quickly converge to the desired range and track the value until they hit the target. This confirmed the effectiveness of the

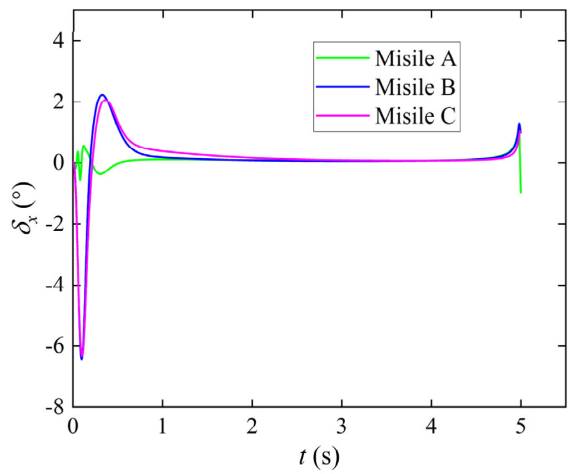

(a)

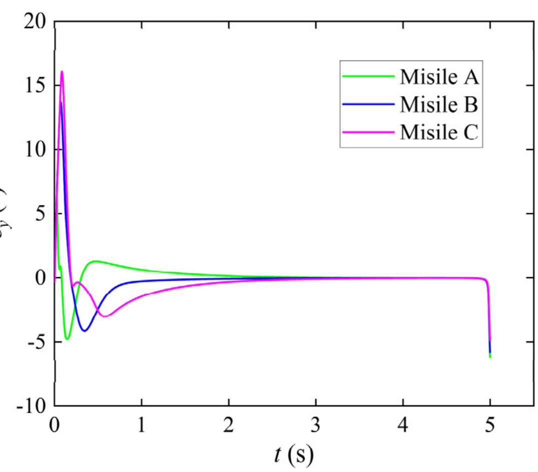

(b)

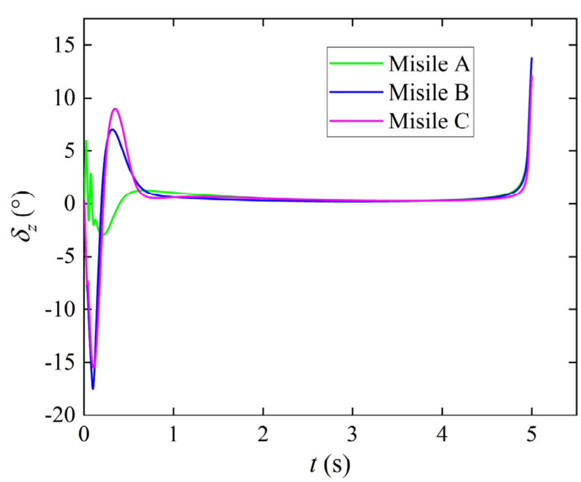

(c)

Fig. 19. Curves of rudder angles δ_x, δ_y, and δ_z for three missiles in Case 2.

Table 4
Simulation results for Case 2.

	T_d (s)	Impact time t_f (s)	q_{2d} (°)	q_{2f} (°)	Miss distance (m)
Missile A	5	4.999	115	115.82	0.8546
Missile B	5	4.999	135	134.90	0.9019
Missile C	5	4.999	160	159.54	0.6482

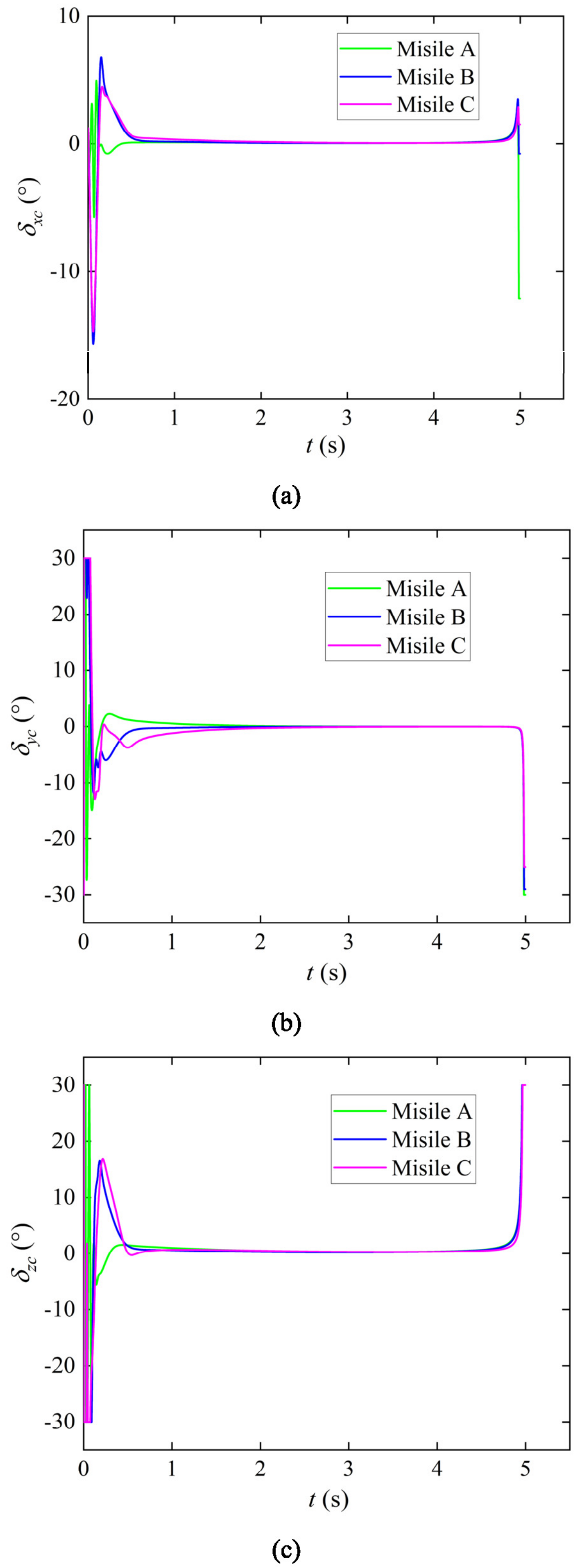

Fig. 20. Curves of control inputs δ_{xc}, δ_{yc}, and δ_{zc} for three missiles in Case 2.

proposed cooperative strategy. Fig. 16 shows that the azimuths of the three missiles can quickly converge to the desired azimuths and continue to follow, further confirming the effectiveness of the proposed ACIGC scheme.

Similar to Case 1, Figs. 17–18 show that the three attitude angles $(\alpha, \beta, \gamma_V)$ and the three angular rates $(\omega_x, \omega_y, \omega_z)$ of the three missiles initially oscillate briefly to adjust the missile flight attitudes to satisfy the attack requirements, but then remain stable. As shown in Fig. 19, the rudder angles of the three missiles did not exceed the maximum rudder angle. Fig. 20 shows that the rudder angle

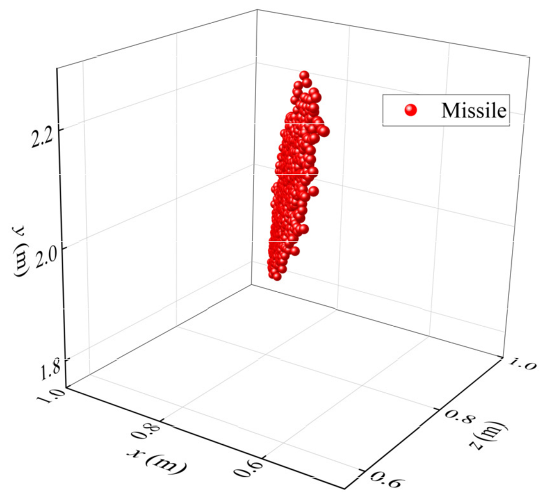

Fig. 21. Interception point distribution of Monte Carlo simulation for Case 3.

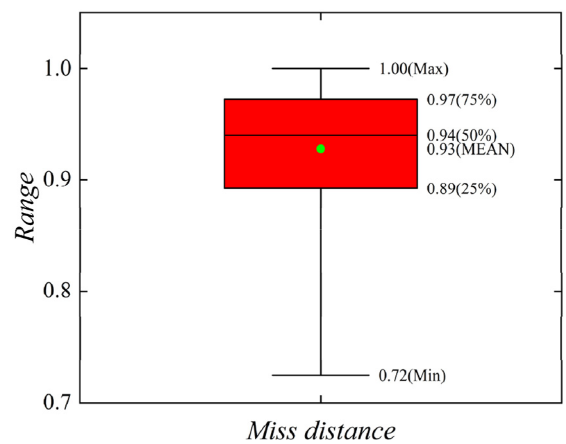

Fig. 22. Missing distance of the Monte Carlo simulation for Case 3.

commands for the pitch and yaw channels of the three missiles initially show saturation inputs but do not last long, indicating that there is still a design margin.

Case 3 *Monte Carlo simulations*

To further demonstrate the robustness of the proposed ACIGC scheme, a Monte Carlo simulation with 1,000 samples was conducted. The aerodynamic force and moment coefficients of the missiles were assumed to deviate randomly by $\pm 20\%$ with respect to the nominal values in each sample. The target makes a sinusoidal maneuver, and the acceleration of the target is taken from $5\sin(\pi t) \sim 15\sin(\pi t)$ m/s^2 randomly in each sample. The velocity of the target is $V_T = 30$ m/s and the initial velocity heading angle $\psi_{VT0} = 0°$. The initial position of the missile is located at a random point in a spherical range of 500 m radius with $(4500, 6000, 5500)$ m as the center of the sphere. The desired impact time is $T_d = 5$ s, and the cooperative coefficient is $\gamma = 1.0$.

The simulation results for 1,000 samples are shown in Figs. 21–23. Fig. 21 depicts the relative missile position distribution at the moment of interception with the target position at the center of the sphere. It can be seen that all intercept points are almost distributed in a longitudinal plane. Fig. 22 shows a box plot of the miss distance, from which it can be seen that the miss distance of all samples is less than 1 m. The average miss distance was 0.93 m, and approximately 50% of them fell within the interval of 0.89–0.97 m. Fig. 23 shows a box plot of the terminal-impact azimuth. It can be observed that the errors between the terminal-impact azimuths and the predefined azimuth of all samples are within 1°, with an average error of 0.35°, and approximately 50% falling within the interval of 0.23–0.42°. In summary, the Monte Carlo simulation results further demonstrated the robustness of the proposed ACIGC scheme for attacking ground-maneuvering targets.

6. Conclusion

Based on the BC, SMC, DSC, and 3D reduced-ESO, this paper proposes a novel three-dimensional ACIGC scheme with fixed-impact azimuth and time constraints for hypersonic STT missiles attacking ground-maneuver targets. The fixed-impact time constraint is achieved by transforming the fixed-impact time into a nominal value of the missile-target range-to-go and by tracking this nominal value. The same impact time only needs to be set at the beginning of the terminal guidance phase. Subsequently, all missiles could simultaneously attack the target without using a communication topology between the missiles. This is helpful for preventing electronic interference from enemy targets, thus improving the penetration probability. Moreover, this enables each missile to attack the target by following its predefined azimuth, thereby further enhancing the destruction effect. In this study, a 3D fifth-order strict-feedback time-varying nonlinear

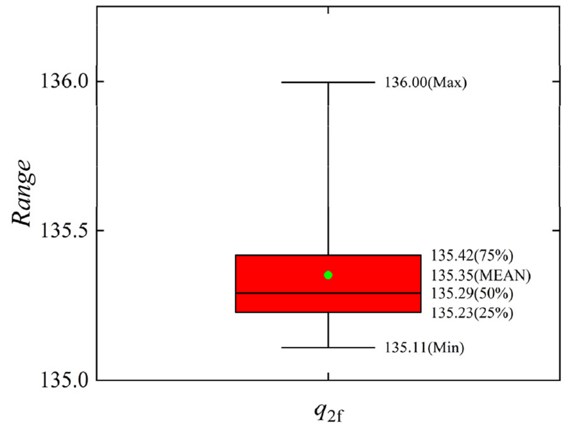

Fig. 23. Terminal-impact azimuths of Monte Carlo simulations for Case 3.

model with mismatched uncertainties was proposed and the system-lumped disturbances were estimated by the 3D reduced-order ESO, which avoided the chattering caused by the introduction of switching terms in the traditional sliding mode control. The proposed ACIGC scheme also considers the saturation constraints and delay dynamics of the rudder, thereby improving its execution. The derivatives of the virtual control commands are obtained using DSC, which solves the "differential explosion" phenomenon caused by BC. Monte Carlo simulations further verify the effectiveness and robustness of the proposed ACIGC scheme.

Hypersonic missiles are required to have a certain terminal maneuvering capability against maneuvering targets, so there are bounding requirements on the missile body attitude. On the basis of this work, the next step is to design an IGC scheme considering system states constraints to achieve system states boundedness, which helps to improve the flight stability of the missile.

Hypersonic missiles besides STT missiles with axisymmetric design, there are also bank-to-turn (BTT) missiles with waverider. The latter adopt the bank-to-turn method for wide-range maneuvering. The IGC model proposed in this paper is based on the small velocity-deflection angle assumption, which is applicable for hypersonic STT missiles to hit ground or sea maneuvering targets, and is not used for BTT missiles. Therefore, the design of CIGC scheme for hypersonic BTT missiles against maneuvering targets on the ground or at the sea needs to be further studied.

Declaration of competing interest

We declare that we have no financial and personal relationships with other people or organizations that can inappropriately influence our work, there is no professional or other personal interest of any nature or kind in any product, service and/or company that could be construed as influencing the position presented in, or the review of, the manuscript entitled.

Data availability

No data was used for the research described in the article.

Appendix A

Nomenclature		V_{Mx}, V_{My}, V_{Mz}	Velocity vectors of the missile in the inertial coordinate system, m/s
m	Mass of the missile, kg	$a_{Mx_L}, a_{My_L}, a_{Mz_L}$	Acceleration vectors of the missile in the LOS coordinate system, m/s^2
g	Gravity acceleration, m/s^2	$a_{tx_L}, a_{ty_L}, a_{tz_L}$	Acceleration vectors of the target in the LOS coordinate system, m/s^2
θ_M, ψ_{VM}	Flight path angle and heading angle of the missile, rad	α, β, γ_V	Angle-of-attack, sideslip angle and velocity-deflection angle, rad
θ_T, ψ_{VT}	Flight path angle and heading angle of the target, rad	ϑ, ψ, γ	Pitch angle, yaw angle and roll angle, rad
q_1, q_2	Elevation and azimuth angles of the line-of-sight, rad	$\delta_x, \delta_y, \delta_z$	Aileron, rudder and elevator deflections, rad
R	Missile-target relative distance, m	$\delta_{xc}, \delta_{yc}, \delta_{zc}$	Control inputs of aileron, rudder and elevator channel, rad
V_M, V_T	Velocity of the missile and target, m/s	J_x, J_y, J_z	Rolling, yawing and pitching moments of inertia, kg/s^2
Q	Dynamic pressure, Pa	$c_y^{\alpha}, c_y^{\beta}, c_y^{\delta_z}$	Lift force coefficient with respect to α, β and δ_z
ρ	Air density, kg/m^3	$c_z^{\alpha}, c_z^{\beta}, c_z^{\delta_y}$	Side force coefficient with respect to α, β and δ_y
S	Reference area, m^2	M_x, M_y, M_z	Roll, yaw, and pitch moments, N·m
L	Reference length, m	$m_x^{\alpha}, m_x^{\beta}, m_x^{\delta_x}$	Rolling moment coefficient with respect to α, β and δ_x
Y, Z	Lift and side forces, N	$m_y^{\beta}, m_y^{\delta_y}$	Yawing moment coefficient with respect to β and δ_y
$\mathbf{R}$	Relative distance vector between the missile and target	$m_z^{\alpha}, m_z^{\delta_z}$	Pitching moment coefficient with respect to α and δ_z
$\mathbf{V_R}$	Relative velocity vector between the missile and target	$\omega_x, \omega_y, \omega_z$	Body-axis roll, yaw and pitch rates, rad/s
$\mathbf{a_R}$	Relative acceleration vector between the missile and target	x_M, y_M, z_M	Position of the missile in inertial frame, m
$\mathbf{\Omega}$	Angular velocity vector of the LOS coordinate system with respect to the inertial coordinate system	x_T, y_T, z_T	Position of the target in inertial frame, m
$V_{Mx_L}, V_{My_L}, V_{Mz_L}$	Velocity vectors of the missile in the LOS coordinate system, m/s	τ_x, τ_y, τ_z	Time constant of the aileron, rudder and elevator channel

References

[1] Y. Ding, X. Yue, G. Chen, J. Si, Review of control and guidance technology on hypersonic vehicle, Chin. J. Aeronaut. 35 (2022) 1–18.
[2] J. In-Soo, L. Jin-Ik, T. Min-Jea, Impact-time-control guidance law for anti-ship missiles, IEEE Trans. Control Syst. Technol. 14 (2006) 260–266.
[3] W. Dong, C. Wang, J. Wang, M. Xin, Varying-gain proportional navigation guidance for precise impact time control, J. Guid. Control Dyn. 46 (2022) 535–552.
[4] H.-G. Kim, H. Lee, Composite guidance for impact time control under physical constraints, IEEE Trans. Aerosp. Electron. Syst. 58 (2022) 1096–1108.
[5] J. Yu, X. Dong, Q. Li, Z. Ren, J. Lv, Cooperative guidance strategy for multiple hypersonic gliding vehicles system, Chin. J. Aeronaut. 33 (2020) 990–1005.
[6] Y. Zhang, X. Wang, H. Wu, Impact time control guidance law with field of view constraint, Aerosp. Sci. Technol. 39 (2014) 361–369.
[7] X. Chen, J. Wang, Optimal control based guidance law to control both impact time and impact angle, Aerosp. Sci. Technol. 84 (2019) 454–463.
[8] X. Chen, J. Wang, Two-stage guidance law with impact time and angle constraints, Nonlinear Dyn. 95 (2019) 2575–2590.
[9] S. Ma, X. Wang, Z. Wang, Field-of-view constrained impact time control guidance via time-varying sliding mode control, Aerospace 8 (2021).
[10] S. He, C. Lee, H. Shin, A. Tsourdos, Optimal three-dimensional impact time guidance with seeker's field-of-view constraint, Chin. J. Aeronaut. 34 (2021) 240–251.
[11] S. Ma, Z. Wang, X. Wang, Q. Chen, Three-dimensional impact time control guidance considering field-of-view constraint and velocity variation, Aerospace 9 (2022).
[12] J. Zhu, D. Su, Y. Xie, H. Sun, Impact time and angle control guidance independent of time-to-go prediction, Aerosp. Sci. Technol. 86 (2019) 818–825.
[13] Z. Hou, Y. Yang, L. Liu, Y. Wang, Terminal sliding mode control based impact time and angle constrained guidance, Aerosp. Sci. Technol. 93 (2019) 105142.
[14] Q. Hu, T. Han, M. Xin, Sliding-mode impact time guidance law design for various target motions, J. Guid. Control Dyn. 42 (2018) 136–148.
[15] J. Zhou, J. Yang, Guidance law design for impact time attack against moving targets, IEEE Trans. Aerosp. Electron. Syst. 54 (2018) 2580–2589.
[16] H. Yu, K. Dai, H. Li, Y. Zou, X. Ma, S. Ma, H. Zhang, Three-dimensional adaptive fixed-time cooperative guidance law with impact time and angle constraints, Aerosp. Sci. Technol. 123 (2022) 107450.
[17] J. Song, S. Song, S. Xu, Three-dimensional cooperative guidance law for multiple missiles with finite-time convergence, Aerosp. Sci. Technol. 67 (2017) 193–205.
[18] J. Zhao, S. Yang, Integrated cooperative guidance framework and cooperative guidance law for multi-missile, Chin. J. Aeronaut. 31 (2018) 546–555.
[19] X. Yang, S. Song, Three-dimensional consensus algorithm for nonsingular distributed cooperative guidance strategy, Aerosp. Sci. Technol. 118 (2021) 106958.
[20] Z. Chen, W. Chen, X. Liu, J. Cheng, Three-dimensional fixed-time robust cooperative guidance law for simultaneous attack with impact angle constraint, Aerosp. Sci. Technol. 110 (2021) 106523.
[21] G. Li, J. Lü, G. Zhu, K. Liu, Distributed observer-based cooperative guidance with appointed impact time and collision avoidance, J. Franklin Inst. 358 (2021) 6976–6993.
[22] C. Ming, X. Wang, R. Sun, A novel non-singular terminal sliding mode control-based integrated missile guidance and control with impact angle constraint, Aerosp. Sci. Technol. 94 (2019) 105368.
[23] Z. Li, Q. Dong, X. Zhang, Y. Gao, Impact angle-constrained integrated guidance and control for supersonic skid-to-turn missiles using backstepping with global fast terminal sliding mode control, Aerosp. Sci. Technol. 122 (2022) 107386.
[24] S. Jiang, F. Tian, S. Sun, W. Liang, Integrated guidance and control of guided projectile with multiple constraints based on fuzzy adaptive and dynamic surface, Def. Technol. 6 (2019) 1130–1141.
[25] A. Sinha, S.R. Kumar, D. Mukherjee, Impact time constrained integrated guidance and control design, Aerosp. Sci. Technol. 115 (2021) 106824.
[26] A. Patil, S.R. Kumar, Integrated impact time guidance and control against non-maneuvering targets, Proc. Inst. Mech. Eng., G J. Aerosp. Eng. 236 (2022) 3327–3343.
[27] A. Sinha, S.R. Kumar, D. Mukherjee, Cooperative integrated guidance and control design for simultaneous interception, Aerosp. Sci. Technol. 120 (2022) 107262.
[28] X. Wang, Y. Zheng, H. Lin, Integrated guidance and control law for cooperative attack of multiple missiles, Aerosp. Sci. Technol. 42 (2015) 1–11.
[29] X. Wang, Y. Zhang, D. Liu, M. He, Three-dimensional cooperative guidance and control law for multiple reentry missiles with time-varying velocities, Aerosp. Sci. Technol. 80 (2018) 127–143.
[30] A. Sinha, S.R. Kumar, D. Mukherjee, Nonsingular impact time guidance and control using deviated pursuit, Aerosp. Sci. Technol. 115 (2021) 106776.
[31] X.H. Wang, C.P. Tan, L.P. Cheng, Impact time and angle constrained integrated guidance and control with application to salvo attack, Asian J. Control 22 (2020) 1211–1220.
[32] C. Ren, X. Lee, X. Yang, S. Ma, Extended state observer-based sliding mode control of an omnidirectional mobile robot with friction compensation, IEEE Trans. Ind. Electron. 66 (2019) 9480–9489.
[33] T. Chao, S. Quan, P. Ma, D. Zhang, Three-dimensional low-order finite-time integrated guidance and control design with side-window constraint, Aerosp. Sci. Technol. 121 (2022) 107355.